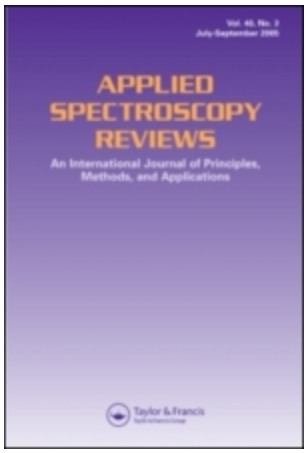

The use of Fourier Transform Infrared (FTIR) Spectroscopy in Skin Cancer Research: A Systematic Review

Journal:	*Applied Spectroscopy Reviews*
Manuscript ID	LAPS-2020-0037.R1
Manuscript Type:	Reviews
Date Submitted by the Author:	30-Jun-2020
Complete List of Authors:	Shakya, Bijay; University of Oulu, Research Unit of Medical Imaging, Physics and Technology Shrestha, Pragya; University of Oulu, Research Unit of Medical Imaging, Physics and Technology Teppo, Hanna-Riikka; University of Oulu, Cancer Research and Translational Medicine Research Unit; Oulu University Hospital, Department of Pathology; Oulu University Hospital and University of Oulu, Medical Research Center Oulu Rieppo, Lassi; University of Oulu, Research Unit of Medical Imaging, Physics and Technology
Keywords:	fourier transform spectroscopy, infra-red spectroscopy, biological

The use of Fourier Transform Infrared (FTIR) Spectroscopy in Skin Cancer Research: A Systematic Review

Bijay Ratna Shakya[a], Pragya Shrestha[a], Hanna-Riikka Teppo[b,c,d], Lassi Rieppo[a*]

[a]*Research Unit of Medical Imaging, Physics and Technology, Faculty of Medicine, University of Oulu, Oulu, Finland*

[b]*Cancer Research and Translational Medicine Research Unit, University of Oulu, Oulu, Finland*

[c]*Department of Pathology, Oulu University Hospital, Oulu, Finland*

[d] *Medical Research Center Oulu, Oulu University Hospital and University of Oulu, Finland*

***Corresponding author**

Lassi Rieppo, Ph.D.

Research Unit of Medical Imaging, Physics and Technology, Faculty of Medicine

University of Oulu

P.O. Box 5000, FI-90014 Oulu, Finland

Email: lassi.rieppo@oulu.fi

Mobile: +358 503759310

Other authors:

Bijay Ratna Shakya: bijay.shakya@oulu.fi

Pragya Shrestha: pragya.shrestha@oulu.fi

Hanna-Riikka Teppo: hanna-riikka.teppo@oulu.fi

The use of Fourier Transform Infrared (FTIR) Spectroscopy in Skin Cancer Research: A Systematic Review

Abstract

Skin cancers are one of the most frequently occurring diseases in humans that pose severe health issues. Fourier Transform Infrared (FTIR) spectroscopy in cancer research has gained considerable attention because of its ability to provide biochemical information in addition to being compatible with traditional histopathology. With this review, we aim to identify all skin cancer studies which have been conducted using FTIR spectroscopy and depict different methodologies that have been used to analyse FTIR spectroscopic data of skin cancers. We conducted the systematic review following PRISMA guidelines for which three databases, Scopus, PubMed and Web of Science, were searched from commencement to 16 January 2019. All the studies which used FTIR spectroscopy for skin cancer research were included in the review. A total of 35 studies were found eligible to be included in the review. Of these, 21 studies were based on melanoma, 6 studies on BCC, 2 studies on SCC, and 2 on lymphocytes. The remaining 4 studies aimed to differentiate between various skin cancer types. The potential of FTIR spectroscopy for many relevant aspects of skin cancer research has already been demonstrated, but more work is needed to establish FTIR spectroscopy as a routine method in the field.

Keywords: skin cancer, melanoma, basal cell carcinoma, squamous cell carcinoma, fourier transform infrared spectroscopy, fourier transform infrared imaging

1. Introduction

The skin is an organised structure formed of three layers: epidermis, dermis and hypodermis. The epidermis is the outermost layer consisting of different cell types. The most abundant cells found in the epidermis are keratinocytes which account for almost 90 to 95% of cells. The remaining 5 to 10 per cent are mainly Langerhans cells, melanocytes and Merkel cells [1]. Skin cancer is the most common of all cancers occurring in humans. It arises due to the uncontrolled growth of abnormal skin cells. Most of the skin cancers are developed from keratinocytes and melanocytes. Keratinocytes form the stratified keratinizing structure of the epidermis, which is responsible for the barrier function between the organism and the environment. Melanocytes, which are found in the basal layer of the epidermis, are derived from the neural crest and are responsible for the production of melanin which forms the skin pigmentation [2].

Ultraviolet radiation is believed to be the major source for inducing skin cancer. It causes DNA damage, gene mutations, immunosuppression, oxidative stress and inflammatory responses which contribute to skin's photoaging, thus making it prone to skin cancer [3,4]. Skin cancers can be divided into two major groups: melanomas and non-melanomas. Non-melanomas comprise the majority of all skin cancers, with basal cell carcinoma (BCC) and squamous cell carcinoma (SCC) being the most common. BCC accounts for almost 80 percent of all non-melanoma skin cancers. Considering its prevalence, the mortality rate of BCC is quite low as it rarely metastasizes, but if left untreated, BCC can cause extensive destruction of tissues with local progression [5]. SCC accounts for approximately 20 percent of non-melanoma cancers. It is the second most common skin cancer and can be treated easily with a high rate of cure, but a minority of lesions may reoccur and metastasize [6]. Melanoma is the third most common type of skin cancer occurring in human. Even though less common than BCC and SCC, melanoma has proven to be the fatal form of skin cancer, causing 80 percent of deaths from skin cancer [7,8]. Thus, the proper diagnosis is crucial for effective clinical intervention.

Most skin cancers can be successfully treated if diagnosed in an early stage. New or suspicious lesions should therefore be clinically assessed and histologically analysed. Current diagnostics of skin cancer is based on histopathology which follows the guidelines of WHO Classification of Skin Tumours [9]. Histological features such as the tumour thickness (Breslow thickness and Clark level), grade of differentiation, ulceration, mitotic rate, vascular invasion, and lymph node involvement, are reported. Histological samples are subjected to an interpretation that is dependent largely on the pathologist's trained eye and experience, aiming at as accurate a diagnostic conclusion as possible. However, histomorphology does not always reflect all the biological features of skin cancer, and therefore histochemical methods, immunostaining techniques and genetic testing are used for supporting diagnosis, differential diagnosis and determining the mutational burden [13,14].

With precise diagnosis and prognostics being a major concern, new approaches and modalities are being actively developed to complement the traditional pathology laboratory methods. Dermoscopy is actively used by dermatologists for improving the diagnostic accuracy of skin cancers. This technique helps in visualization of morphological structures of superficial skin [15]. Other optical techniques, such as optical coherence tomography, fluorescence spectrometry, reflectance spectrometry, Raman spectroscopy and confocal microscopy, have also shown to be promising in improving diagnostic accuracy, but these methods are not yet in clinical use [16]. Lately, Fourier Transform Infrared (FTIR) spectroscopy have gained considerable attention due to its versatility in detecting biochemical and biological features present in the samples. The detection is based on the absorption of mid-infrared (400-4000 cm^{-1}) light by the sample. The absorption spectrum consists of various peaks at different wavenumbers depending on the vibrational modes of each molecule present within the sample. The intensities and positions of these peaks depend on the biochemical molecules (e.g. proteins, lipids and nucleic acids), the structure and conformation of these molecules and their

intermolecular relationships [17]. This information can be used to distinguish cell types, healthy and diseased condition, tumour aggressiveness and to obtain additional prognostic information. Therefore, FTIR spectroscopy has been recognized as an emerging tool for histopathological studies [18-20]. With this systematic review, we aim to identify all skin cancer studies which have been conducted using FTIR spectroscopy. This will help to evaluate the potential of FTIR spectroscopy in skin cancer research and depict different methodologies that have been used to analyse FTIR spectroscopic data, thus conveying the current state of the art in the field.

2. Methods

This systematic review was conducted following the guidelines reported by the Preferred Reporting Items for Systematic Reviews and Meta-Analyses (PRISMA, http://www.prisma-statement.org/).

2.1 Eligibility Criteria

We included only peer-reviewed journal articles in which FTIR spectroscopy was used to acquire data on skin cancers. However, there was no sample-type limitation. All articles using cells, tissues, blood or serum as a sample from humans and animals were included. In case the article has studied multiple cancer types, the study was included if separate samples were used to investigate skin cancer.

Studies were excluded based on the following exclusion criteria: (i) studies related to epithelial carcinomas from other body parts (e.g. laryngeal, vulval, etc.); (ii) studies focusing on skin fibroblast cells; (iii) studies based on self-designed probe or sensor; (iv) articles published in conference proceedings; (v) studies with no originality; (vi) studies comprising of the same dataset; (vii) review articles.

2.2 Information Sources

We searched three electronic databases for this review: Scopus, PubMed and Web of Science. The following keywords were used for searching the relevant articles: [("infrared spectroscopy" OR "Fourier transform infrared spectroscopy" OR "FTIR" OR "attenuated total reflection" OR "ATR") AND ("skin cancer" OR "melanoma" OR "basal cell carcinoma" OR "BCC" OR "squamous cell carcinoma" OR "SCC" OR "Merkel cells" OR "skin lymphoma")]. The search results were limited to English language articles. Each database was searched from commencement to 16 January 2019.

2.3 Study Selection

Keywords used for searching the related articles were defined and validated by all authors (BRS, PS, HRT, LR). The initial search and screening of the titles and abstracts of all articles identified by the keywords were performed by one author (BRS) to exclude articles that were not relevant according to the eligibility criteria. Initially, a total of 1529 articles were generated from three electronic databases. This was reduced to 937 articles after removal of duplicates. After the screening of the titles and abstracts, 884 articles were excluded from the review. The remaining 53 articles were read in full-text by two authors (BRS and PS) working independently in order to assess their suitability for inclusion in this review using predefined criteria. Confusion concerning inclusion/exclusion of the articles was resolved by discussion with another author (LR). Finally, out of 53 full-text articles, 35 articles were considered eligible for inclusion in this review.

2.4 Data Collection Process and Items

The data from the selected articles were collected by one author (BRS) which included the following information: article information (author, year of publication), sample characteristics (sample origin, sample type, sample arrangement, thickness, substrate used), disease type (melanoma, BCC, SCC), number of samples, mode of measurement, utilized absorption bands, pre-processing methods, software tools used, employed algorithms and final outcome of the articles. Two authors (PS and LR) cross-checked all the retrieved information while another author (HRT) cross-checked the biological information.

3. Results

3.1 Study selection

The detailed procedure for identification, inclusion and exclusion of the studies for this review is shown in Figure 1, while the detailed description of all the studies included in this review is shown in Table 1.

3.2 Study Characteristics

3.2.1 Study Information

Out of 35 studies included in the review, 21 studies were based on melanoma. Among them, two studies were based on predicting the effectiveness of drugs to melanoma cells, and three of them were based on differentiating drug-resistant and drug-sensitive melanoma cells. Six studies were based on BCC, two on SCC, and two on lymphocytes. The remaining four studies were based on differentiating between various skin cancer types. No studies based on Merkel cell carcinoma and skin lymphoma were found during study selection.

3.2.2 Sample Information

Samples originating from human sources were used in most of the studies (n = 29), with mice (n = 3) being the second most common source of samples. Additionally, two studies used both humans and mice, while one study was based on engineered tissue. Biopsies were the most commonly used sample type (n = 20) for the spectroscopic measurement, followed by cell cultures (one study cultured cells on the top of a 3D Myoma disc) (n = 9), blood (n = 4), serum (n = 1) and engineered tissue (n = 1). Formalin-fixed paraffin-embedded (FFPE) samples were used in 21 studies, among which 16 studies deparaffinised the samples prior to measurement, five studies used FFPE samples without deparaffinisation, and one study used only formalin-fixed samples without paraffin embedding. In six studies, samples were dried on the used substrate, and in five studies, samples were placed directly onto ATR crystal. In one study,

tissue samples were placed in powdered α-quartz, while in another, tissue samples were placed on KBr pellets.

3.2.3 Mode of Measurement

Spectroscopic data of the samples were acquired using transmission mode in 22 studies, transflection mode in three studies, both (transmission and transflection) in one study, and ATR in nine studies. Generally, the samples were placed on substrates like BaF_2, CaF_2 or ZnSe for transmission mode measurements. Low emissivity slides were used for transflection mode, and diamond, ZnSe, and Ge were used as crystals for ATR measurements. Figure 2 shows an overview of the spectral acquisition using different measurement modes.

3.2.4 Pre-processing

Of the eligible 35 studies, 30 studies carried out the pre-processing of acquired spectroscopic data before the analysis. In the remaining 5 studies, no information about pre-processing is given. Normalization (n = 26), baseline correction (n = 16), water vapour correction (n = 10), carbon dioxide peak removal (n = 9), second derivative (n = 7), extended multiplicative signal correction algorithm (EMSC) (n = 6), Savitzky-Golay filter (n = 4), PCA (n = 3) and standard normal variate (n = 1) were used as pre-processing procedures in included studies.

3.2.5 Algorithms

Almost all the studies have used more than one algorithm for the analysis of spectral data. Cluster analysis (K-means clustering, hierarchical clustering, unsupervised hierarchical clustering, hybrid hierarchical agglomerative clustering, fuzzy C-means clustering) was the most commonly used algorithm in the included studies (n = 16), followed by principal component analysis (PCA) (n=12), discriminant analysis (linear discriminant analysis, quadratic discriminant analysis, partial least square discriminant analysis (PLS-DA)) (n = 10), univariate analysis (n = 10), partial least square regression (PLSR) (n = 2), deconvolution (n =

2), and discriminant classification function (n = 2). Other algorithms, including a computational model based on density functional theory (STmod), soft independent modelling class analogy (SIMCA), and artificial neural network (ANN), were used in three separate studies independently. Additionally, statistical analysis, including t-test, analysis of variance (ANOVA), multivariate analysis of variance (MANOVA), comprehensive data map (CDM) and SM-MATLAB (a model based on Gaussian distribution and posterior probabilities), were carried out in eighteen studies.

3.3 Melanoma Research

Twenty-one studies (60%) included in this review investigated melanoma using FTIR spectroscopy. Among these studies, four were based on differentiating melanoma from healthy or non-tumoral samples [21-24]. Five studies investigated various skin lesions (i.e. nevi and melanomas) with respect to normal skin to differentiate between them based on biochemical changes occurring with the condition [25-29]. One study investigated spectral differences between various histological melanoma subtypes [30]. According to this study, FTIR imaging can separate melanomas from normal epidermal structures, identify spectroscopic markers of melanoma cells with differences in cell morphology and characterize intratumoral heterogeneity of different tumour types. This study also suggests a good correlation between the heterogeneity reflected in the presence of several infrared clusters of primary cutaneous melanomas and dermatopathological parameters, such as Breslow thickness, Clark level, ulceration and mitotic index.

Two studies were based on identifying the major cell types and structures (pigment cells, keratinocytes, lymphocytes and erythrocytes, connective tissue structures, necrotic cells) present in melanoma samples [31,32]. The former dealt with primary melanoma samples, comparing the infrared spectra of primary tumours diagnosed at different stages of disease,

suggesting that the presence of metastases can be predicted from the spectral signature of primary melanomas. The latter one studied melanoma metastases in lymph nodes, and in addition to identifying main cell types, it also suggested the possibility to identify the presence of metastases through the impact they have on lymphocytes. One more study associated with determining the metastatic potential of melanoma cells focused on the intermolecular structure of water molecules revealed a higher level of fluidity in the plasma membrane of metastatic cells, which results in higher plasma membrane hydration level compared to non-metastatic cells [33].

One study showed that the 3D myoma model together with FTIR spectroscopy can provide a biologically relevant system for cancer invasion research by analysing changes in tissue microenvironment [34], while another study has shown engineered tissue can be used as a model for monitoring disease progression and phantoms for imaging [35].

FFPE processed samples are routinely used in tissue research. One study reported that the use of FFPE processing during sample preparation can cause small but significant changes in cell infrared spectra. The loss of phospholipids and noticeable change in protein secondary structure following FFPE treatment are the reasons for these modifications. However, distinctions between infrared spectra of cellular subtypes are reported as being as accurate as prior to FFPE processing [36].

Five studies were based on predicting the response of melanoma cells to drugs. Among them, three studies showed that drug-resistant and drug-sensitive melanoma cells can be differentiated using FTIR spectroscopy, even though these cells are morphologically indistinguishable [37-39]. One study demonstrated that boric acid supplementation affects both the morphological and chemical composition of melanoma cells and, furthermore, suggested that high concentrations of boric acid have an anti-proliferative effect and show signs consistent

with apoptosis [40]. Another study determined anti-melanogenic activity caused in melanoma cells due to sesamol and kojic acid. The study suggested that sesamol acts by inhibiting tyrosinase activity which results in decreased melanin content and possesses stronger anti-melanogenesis than kojic acid [41].

3.4 BCC Research

Six studies (17%) included in this review investigated BCC. Among them, three studies used FTIR spectra of blood samples to discriminate between healthy and those affected with BCC [42-44]. One study applied FTIR spectroscopy combined with high pressure to differentiate BCC and normal skin samples [45]. High-pressure studies were performed by applying small amounts of tissue samples at room temperature together with powdered α-quartz in a stainless-steel gasket mounted on a diamond anvil cell. One study used FFPE samples to successfully identify the tumour lesions from infrared spectral images of tissue sections without dewaxing the paraffin [46]. One other study also used FFPE samples to identify the changes in FTIR spectra due to the development of BCC, in order to differentiate BCC from other skin lesions (melanocytic and SCC), and to distinguish different subtypes of BBC based on the acquired spectra [47].

3.5 SCC Research

Two studies (6%) included in this review investigated SCC. One study used first-principles density functional theory-based vibrational calculations to analyse the differences in the FTIR spectra in SCC and normal tissue. The study suggested that protonated proline is responsible for the strong coupling between vibrations in the amide region, and that proline plays a significant role in tumorogenesis [48]. Other studies have assessed the biochemical changes in the normal skin caused by the development of SCC induced by multistage chemical

carcinogenesis, and showed that the differences between them are mainly seen in the wavenumbers associated with protein content [49].

3.6 Combined Research

Four studies (11%) in this review investigated more than one cancer type in the same study to assess the capability of FTIR spectroscopy for the differential diagnosis of skin cancers. Among them, two studies used different carcinoma samples (SCC, BCC, Bowen's disease) and healthy samples to show the potential of FTIR spectroscopy in differentiating normal skin from disease as well as differentiating between various carcinoma samples [50,51]. One study used same carcinoma samples and focused on developing the algorithm for determining optimal fuzzy C-means parameters (number of clusters and fuzziness index), making the algorithm more powerful to reveal biologically relevant information related to tumour heterogeneity and invasiveness [52]. The final study used BCC, melanoma and nevus as their research samples and showed the spectral differences occurring with each condition [53]. In addition, the study also suggested using the band arising from hyaluronic acid as a "marker band" of melanoma as it may discriminate melanoma from non-melanoma cancers due to the presence of many hyaluronic acid chain breakages.

3.7 Lymphocyte Research

One FTIR imaging study conducted on lymphocyte subpopulations [54] showed the ability of FTIR imaging in accurately identifying cytotoxic T cells (CD8+), helper T cells (CD4+) and in quantifying regulatory T cells (CD25+) among a mix of other cell types from human blood samples. Another study demonstrated the ability of FTIR imaging to detect the presence of human leukocyte antigen (HLA) class I from FFPE tissue samples without the need for antibody attachment [55].

3.8 Infrared Spectra of Skin Components

An example of a melanoma cell FTIR spectrum showing prominent bands associated with skin cancer diagnosis is shown in ~~figure~~ Figure ~~2~~3. Nucleic acids, carbohydrates and phosphates mainly absorb in the region of 900–1300 cm^{-1} and have many overlapping vibrational modes associated with them, including RNA at 1244, 1121 and 996 cm^{-1}, and DNA at 1230, 1020 and 966 cm^{-1} [21,23,25,28]. The band near 1080 cm^{-1} arises due to the vibration of symmetric phosphate [$v_s(PO_2-)$] [21,23,28,42], and the band at 1056 cm^{-1} corresponds to the $v_s(PO_2-)$ absorbance of phosphodiesters of nucleic acids and the O-H stretching coupled with C-O bending of C-OH groups of carbohydrates [23,37,38]. Absorbance bands near 1033 cm^{-1} and 1076 cm^{-1} are due to the presence of glucose (C-O stretching carbohydrate, β-anomer) and mannose (C-O stretching carbohydrate α-anomer) [23]. The band near 1238 cm^{-1} arises due to antisymmetric vibration of phosphate [v_{as} (PO_2-)] [21,23,25,28,42].

In the region of 1300-1500cm^{-1}, absorbance mainly occurs due to vibrational modes arising from residues of amino acids along with stretching and bending modes of membrane lipids. One of the bands in this region occurs at 1456 cm^{-1} which consists of overlapping bands at 1464 cm^{-1}, 1456 cm^{-1} arising due to symmetric bending of CH_2 in lipids [δ_s (CH_2)] and 1446 cm^{-1} arising due to antisymmetric bending of CH_3 in lipids [δ_{as} (CH_3)]. The other band occurs at 1400 cm^{-1} which arises due to the symmetric vibrations of carboxylate functional groups in proteins [v_s (C=O)] [38,41,42].

Absorption in the region between 1500–1750 cm^{-1} occurs mostly due to vibrations in proteins and nucleic acids. The two main bands in this region are amide I, which is due to amide C=O stretching, and amide II, which is mostly due to amide N-H stretching [23,25,28,39,42]. The amide I band comprises several major absorption bands which are associated with the secondary structure of proteins [23,28,38,41]. Tyrosine, an amino acid, has a band at the wavenumbers between 1512–1515cm^{-1}. Tyrosine is considered important metabolite as its level changes significantly during skin malignancy or development of melanoma [21]. Though phosphates of

nucleic acids predominantly absorb between 900–1300 cm^{-1}, the bases of nucleic acids absorb also in the amide I and amide II regions. These nucleic acid bases include adenine (1682 cm^{-1}), guanine (1633 cm^{-1}), uracil (1622 cm^{-1}), thymine (1576 cm^{-1}) and cytosine (1536 cm^{-1}). These bands arise from the C–N and C–O bonds in nucleic acids [21].

Absorption in the region between 2800–3000 cm^{-1} occurs mainly due to lipids. There are four prominent absorbance bands in this region. The first one at 2852 cm^{-1} is due to the symmetric stretching of the methylene chains in membrane lipids, the second at 2871 cm^{-1} arises from the symmetric CH_3 (methyl) stretching, the third at 2923 cm^{-1} is due to the antisymmetric CH_2 stretch, and fourth at 2958 cm^{-1} is due to antisymmetric stretching of the methyl groups of both lipids and proteins [25,37-39,41]. The detailed description of bands along with associated wavenumbers and bonds are shown in table 2.

Presented are approximate band positions which may vary depending on the type of sample used, the sample preparation method, and the mode of measurement. Figure 4 displays slight differences in melanoma cell spectra acquired using different measurement modes.

3.9 Spectroscopic characteristics

3.9.1 Melanoma

Most studies have focused on the fingerprint region, i.e., 900-1800 cm^{-1}, as it shows the most visible differences among various parameters. Figure 5 shows the fingerprint region spectra of melanoma cells and healthy skin cells acquired from a histological skin section. The parameters derived from the nucleic acid, tyrosine, protein and phosphate bands can be used to differentiate melanoma from normal epidermis [21,23]. These parameters include ratios such as RNA/DNA, cytosine+guanine/total (where 'total' is the sum of the absorbance intensities due to nucleic acid bases adenine, guanine, thymine and cytosine), thymine/amide II, amide I/amide II and tyrosine/amide II. Moreover, the peak shifts of amide I and antisymmetric phosphate bands can

be considered as additional indicators for the distinction between melanoma and normal epidermis.

The symmetric phosphate absorbance may be used to differentiate melanoma from nevus. Compared with normal epidermis, the amide I band shifts to a lower wavenumber in the case of melanoma and to a higher wavenumber in the case of nevus. This shift can act as a distinguishing feature between melanoma and nevus. The CH_2 antisymmetric stretching band also shifts to a lower wavenumber in the case of nevus and to a higher wavenumber in the case of melanoma [25]. The RNA/DNA ratio may not be considered reliable when differentiating melanoma and nevus. One study reported lower RNA/DNA ratio in nevus and melanoma when compared with normal epidermis, but two other studies reported higher RNA/DNA ratio in malignant areas compared with normal areas [25,26,29]. RNA/DNA ratio may have value as a spectral biomarker for discriminating drug-resistant and drug-sensitive melanoma cells. Along with this ratio, ν_{as} CH_3/ν_s CH_2, lipid/protein ratio and amide I are also promising biomarkers for drug sensitivity [37,38]. One study defined spectral markers for discriminating different typologies of melanocytes which include (i) the increase of ν_{c-o} non H-bonded/ν_{c-o} H-bonded and glycogen/amide II in classic spitzoid melanocytes; (ii) the increase of helical/β-structures, ν_{asym} CH_2/ ν_{asym} CH_3, and ν = CH/ ν_{asym} CH_3, together with the decrease of glycogen/amide II in desmoplastic and atypical spitzoid melanocytes [29].

Supervised methods, such as PLS-DA, can be used for identification of main cell types, including melanoma cells, found in skin biopsies and lymph nodes invaded by melanoma. PLS-DA has also been used to differentiate primary tumours between non-metastatic and metastatic stages, identify lymphocyte subpopulations (T cells and B cells), discriminate lymphocytes present in invaded or non-invaded lymph node, and differentiate drug-sensitive and drug-resistant melanoma cells with high sensitivity and specificity [31,32,39]. PCA, an unsupervised method, provided good separation between the spectra extracted from different regions of

myoma tissue, e.g. close to the tumour cells, middle of tissue, and far from the tumour cells, which can aid to understand the influence of cancer cells on surrounding tumour microenvironment [34]. Separation of drug-resistant and drug-sensitive melanoma cells can also be achieved using PCA to anticipate the response to defined treatment [37,39].

3.9.2 Non-melanoma skin cancers

Among non-melanoma cancers, compared to normal epidermis, the main spectral characteristics of BCC are increased hydrogen bonding of the phosphodiester group of nucleic acids, decreased hydrogen bonding of the C–OH groups of proteins, increased intensity of the bands at 972, 1080 and 1240 cm^{-1}, decreased intensity ratio of CH_3 stretching band to CH_2 stretching band, and accumulation of unidentified carbohydrates, some of which are specifically observed only in BCC [44,45,47].

The changes observed in SCC are mainly seen in the protein region. There is increase in intensity related to amide I and amide II regions including shift of peaks related to the sub-bands associated with amide II region compared to that of normal tissue [48,49].

4. Discussion

This systematic review of 35 published studies investigated the work that has been carried out in the skin cancer field using FTIR spectroscopy. The results of this review show that research in skin neoplasms is mostly focused on melanoma, but non-melanoma cancers have also been studied. The challenging histopathology of pigment cell tumours, aggressiveness of melanoma and the high mortality rate associated with melanoma are likely the reasons for this focus. Due to the heterogenous nature of the samples, parameters and methodologies reviewed in this paper, conclusive evidence on the most appropriate spectroscopic biomarkers for discriminating between different skin cancer cells and healthy cells is difficult to provide.

The included studies consist of various types of samples (biopsies, cell lines, blood, serum). This highlights the flexibility and capability of FTIR spectroscopy in working with different sample types and different fixation, embedding and mounting methods, establishing it as an emerging tool for histopathological and cytopathological studies. A study by Peñaranda et al. [24] demonstrated the strong influence of sample preparation on the results and comparability of cell spectra acquired using FTIR microscopy. It also stressed the importance of the development of standard FTIR protocols that should be adapted in the existing routine procedures of biomedical laboratories, as most diagnostic samples are preserved and archived in paraffin blocks. Five studies [27,30,46,50,52] actually used samples without deparaffinization, which indicates that the FTIR spectroscopic approach would not waste any of the valuable tissue material, since the section could be reused thereafter in routine staining. As a method deviating from conventional laboratory routine, Kyriakidou et al. [53] studied formalin-fixed tissues without paraffin embedding, because the dewaxing process alters the detection of lipophilic soluble products and aggregates initiated and produced during the development of cancer.

FTIR spectroscopy is useful in the detection of biochemical properties on a cellular level. It is able to differentiate between cells in different cell cycles, cells that are only a few hours apart within the cell cycle, and apoptotic cells based on the biochemical changes occurring during various phases of the cell cycle [56,57], and it can also extract information from the cytological appearance of cells [30]. Furthermore, it can be used to study plasma membrane alterations [33,53] and accumulation of substances such as pigment, amyloid, hyaluronic acid and collagen [53]. Also, changes based on oxidative stress can be detected, for instance in the form of lipid peroxidation [53]. In an experimental setting, the addition of copious amounts of 30% H_2O_2 on the normal skin cells can produce similar peak shifts in the spectra acquired from FTIR spectroscopy to those seen in malignant cells [22]. This suggests that the change in FTIR spectra in malignancy may be due to the presence of high endogenous levels of oxidizers.

As a promising tool for pathologists, FTIR spectroscopy can discriminate epidermal structures from dermis based on the effect of dermal collagen, melanocytes from keratinocytes based on nucleic acid composition and other adnexal structures embedded in the dermis. It can also make a distinction between benign, dysplastic and malignant melanocytes as well as melanophages based on second derivate spectra [21,28]. It is able to discriminate normal skin, malignant melanoma and spitzoid histology based on PCA analysis and spectral changes reflecting from altered protein and nucleic acid structures and high glycogen content in malignant cells [29]. To support the morphological assessment of melanomatous lesions, the tumour environment and different subpopulations of lymphocytes (T cells and B cells), a visual representation with K-means clustering could be a potential analysis tool [30,32]. Tfayli et al. [27] highlighted the importance of proper spectral zone selection in FTIR spectra during hierarchical classification as this plays a major role in influencing the results of clustering. They suggested that four spectral zones combined, corresponding to DNA and melanin vibrations, can help in discriminating melanoma from nevi.

Tissue microenvironment plays a major role during migration as it provides nourishment to the cancer cells during proliferation. It is also an active participant during each step of carcinogenesis leading to metastases, where cells detach themselves from the primary tumour site and migrate through the blood and lymphatic nodes to distant sites within the body [58]. A study by Ukkonen et al. [34] showed these biochemical changes in the tissue microenvironment can be effectively detected by FTIR imaging, and the features present in the amide and collagen triplet region can serve as spectral markers for cancer-induced modification in the tissue microenvironment. This was also verified in the study by Kong et al. [35] in which they used engineered tissue to monitor the progression of melanoma cells over a certain period of time. They also found that the region closer to the tumour undergoes spectral changes that reflect the underlying change of biomolecular expression, suggesting the possibility of heterotypic interactions and transformations in engineered tissue. This study also highlights the advantage of using engineered tissue for cancer research as well as in quality control and standardization in tissue engineering.

Metastasis of melanoma is responsible for the majority of the skin cancer-related deaths. Therefore, an accurate diagnosis is necessary for adjuvant treatment and the treatment of metastatic disease. Apart from the pathological characteristics described in the TNM classification of melanoma, currently no biomarkers are available for assessing the risk of metastasis based on the primary melanoma [59,60]. Three studies aimed to characterize the metastatic potential of melanoma cells using FTIR spectroscopy. Two studies by Wald et al. [31,32] identified major cell types found in primary melanomas and metastatic melanomas through FTIR imaging and compared the spectra of primary melanoma cells with those of metastatic cells. In the first study, they were not able to differentiate between the FTIR spectra of melanoma cells in the primary tumour and metastases. However, they were able to differentiate between the primary tumours of patients at stage I or II from those at stage III or

IV, indicating the possibility of identifying cells in the primary lesion that demonstrate metastatic potential. In the second study, they worked specifically on melanoma cells and different subpopulations of lymphocytes from the lymph node invaded by melanoma as these cells play an active role in tumour reduction. The result of this study suggested that the presence of metastases can be identified through the impact they have on lymphocytes. FTIR spectra from surrounding lymphocytes would, therefore, serve as a convenient surrogate marker for metastasis in diagnostic histopathology, considering that careful dissection of resected lymph nodes is tedious and might result in missing small metastatic clusters of melanoma cells despite serial sectioning and immunohistochemical staining. Also, higher hydration levels in plasma membrane could serve as a marker for the metastatic capacity of the tumour cells [33].

Once the tumour metastasizes, treatment becomes difficult as treatment options like chemotherapy and radiotherapy do not demonstrate a high response rate in melanoma due to its intrinsic resistance to anti-cancer drugs and ionizing radiation. FTIR spectroscopy has shown the ability to determine the effectiveness of the used drugs, and it is also able to differentiate between morphologically indistinguishable drug-resistant and drug-sensitive melanoma cells [37-39]. Moreover, FTIR imaging was also used for the determination of anti-melanogenic activity. It successfully demonstrated the anti-proliferative effect of boric acid on melanoma cells showing signs consistent with apoptosis [40]. FTIR spectroscopy was also used to study the anti-melanogenic activity in melanoma cells due to sesamol and kojic acid [41]. The study illustrated that sesamol, which inhibits the tyrosinase activity resulting in decreased melanin content, possesses a stronger anti-melanogenic effect than kojic acid.

Tumour infiltrating lymphocytes in the primary tumour and in metastases of melanoma patients have shown positive correlation with successful immunotherapy. Therefore, it is important to identify, quantify and characterize immune infiltration at the tumour site for better diagnostics and help in choosing the most efficacious treatment. The capability of FTIR imaging in

identifying different lymphocyte subpopulations, namely the cytotoxic T cells (CD8+), the helper T cells (CD4+) and the regulatory T cells (CD25+), has been demonstrated [54]. This result highlights the sensitivity of FTIR imaging in detecting low biological variability observed in T cell subpopulations which can assist in successful immunotherapy. Additionally, FTIR imaging also enables the distinction of human leukocyte antigen (HLA) class I positive, and negative areas in melanomas without being facilitated by any antibody attachment, which comprises most of the cost in immunohistochemical staining [55].

Non-melanoma cancers encompass carcinomas that usually grow slowly and invade locally around the site. Studies have been carried out to differentiate non-melanoma cancers from normal skin. Wong et al. [45] have shown that FTIR spectra of BCC combined with high pressure differ dramatically from those of normal skin based on alterations in the nucleic acid and protein molecules and accumulation of carbohydrates. Khanmohammadi et al. [42-44] have investigated various algorithms and shown their capabilities in discriminating FTIR spectra of healthy people from those affected with BCC. Furthermore, McIntosh et al. [47] successfully separated FTIR spectra of BCC from the epidermis, follicle sheath, and also the epidermis overlying BCC from normal tissue, which indicated changes in the biochemistry of the epidermis with tumour progression. In addition, they were able to separate BCC, SCC and melanocytic lesions based on the DNA structure but were less successful in classifying BCC subtypes. Ly et al. [46] have shown FTIR imaging is sensitive enough for the identification of BCC lesions within a complex tissue structure and suggested the combined use of EMSC with cluster analysis for this purpose.

Among non-melanoma cancers, SCC is more aggressive and has the ability of metastatic growth. Lima et al. [49] have shown that the differences in neoplastic lesions and normal tissue mostly occur in the wavenumbers associated with protein content, and good classification can be achieved between the two groups based on the spectra acquired using ATR-FTIR. Bortoletto

et al. [48] also investigated the protein region (specifically the amide band region) of the FTIR spectra of SCC and healthy tissues acquired with ATR, and concluded that strong coupling between vibrations occurring in this region due to tumorogenesis is mainly the result of using protonated proline instead of water.

5. Conclusion

This review summarizes the research that has been carried out on skin cancer using FTIR spectroscopy. FTIR spectroscopy is capable of differentiating healthy or normal samples from melanoma and non-melanoma samples with a high degree of accuracy. Moreover, it is also able to differentiate between melanoma and non-melanoma skin cancers, as well as between the most common non-melanoma skin cancers. Additionally, it can characterize the metastatic potential of tumour cells. It possesses the ability to predict the effectiveness of drugs on tumour cells and can identify and quantify different subpopulations of T cells, a factor which can aid successful immunotherapy, with or without the addition of any antibody. As a result of this, we can conclude that FTIR spectroscopy has evolved as a powerful tool for histopathological and cytopathological studies. Having the advantage of being non-destructive and requiring little sample preparation, it has gained popularity among researchers for the analysis of biological samples. Giving detailed information on the biochemical contents of cells and tissues, it is indeed an intriguing methodological approach for biochemical research. However, there is currently only a limited amount of skin cancer FTIR spectroscopy studies. The previous studies are mainly focused on differentiating skin cancers from healthy tissues, and therefore, future studies should aim to provide additional prognostic and predictive information of skin cancers based on FTIR spectra. Furthermore, studies on the development of standard FTIR spectroscopy protocols should be carried out and adapted in future studies to enable easier comparison between the studies conducted in different laboratories. The potential of FTIR spectroscopy for many relevant aspects of skin cancer research has been demonstrated, but

more work is needed to establish FTIR spectroscopy as a routine method in the field of skin cancer research and diagnostics.

6. Acknowledgments

-

7. Declaration of interest

No conflicts of interest.

References

[1] Kanitakis, J. Anatomy, histology and immunohistochemistry of normal human skin. *European journal of dermatology* **2002**, *12*, 390-401.

[2] Haake, A.; Scott, G. A.; Holbrook, K. A. Structure and function of the skin: overview of the epidermis and dermis. In *The biology of the skin*; Freinkel, R. K., Woodley, D. T., Eds.; Parthenon Publishing: New York, London, 2001; pp 19-45.

[3] Narayanan, D. L.; Saladi, R. N.; Fox, J. L. Ultraviolet radiation and skin cancer. *Int. J. Dermatol.* **2010**, *49*, 978-986.

[4] Madan, V.; Lear, J. T.; Szeimies, R. Non-melanoma skin cancer. *The lancet* **2010**, *375*, 673-685.

[5] Ting, P. T.; Kasper, R.; Arlette, J. P. Metastatic basal cell carcinoma: report of two cases and literature review. *J. Cutan. Med. Surg.* **2005**, *9*, 10-15.

[6] Brougham, N. D.; Tan, S. T. The incidence and risk factors of metastasis for cutaneous squamous cell carcinoma—implications on the T-classification system. *J. Surg. Oncol.* **2014**, *110*, 876-882.

[7] Siegel, R.; Naishadham, D.; Jemal, A. Cancer statistics, 2013. *CA: a cancer journal for clinicians* **2013**, *63*, 11-30.

[8] Miller, A. J.; Mihm Jr, M. C. Melanoma. *N. Engl. J. Med.* **2006**, *355*, 51-65.

[9] Elder, D. E.; Massi, D.; Scolyer, R. A.; Willemze, R. *WHO classification of skin tumours;* International Agency for Research on Cancer: 2018; .

[10] Rigel, D. S.; Friedman, R. J.; Kopf, A. W.; Polsky, D. ABCDE—an evolving concept in the early detection of melanoma. *Arch. Dermatol.* **2005**, *141*, 1032-1034.

[11] Goulart, J. M.; Malvehy, J.; Puig, S.; Martin, G.; Marghoob, A. A. Dermoscopy in skin self-examination: a useful tool for select patients. *Arch. Dermatol.* **2011**, *147*, 53-58.

[12] Helsing, P.; Loeb, M. Small diameter melanoma: a follow-up of the Norwegian Melanoma Project. *Br. J. Dermatol.* **2004**, *151*, 1081-1083.

[13] Timar, J.; Vizkeleti, L.; Doma, V.; Barbai, T.; Raso, E. Genetic progression of malignant melanoma. *Cancer Metastasis Rev.* **2016**, *35*, 93-107.

[14] Alhumaidi, A. Practical immunohistochemistry of epithelial skin tumor. *Indian J. Dermatol. Venereol. Leprol.* **2012**, *78*, 698-708. DOI: 10.4103/0378-6323.102359 [doi].

[15] Argenziano, G.; Soyer, H. P. Dermoscopy of pigmented skin lesions–a valuable tool for early. *The lancet oncology* **2001**, *2*, 443-449.

[16] Calin, M. A.; Parasca, S. V.; Savastru, R.; Calin, M. R.; Dontu, S. Optical techniques for the noninvasive diagnosis of skin cancer. *J. Cancer Res. Clin. Oncol.* **2013**, *139*, 1083-1104.

[17] Stuart, B. Infrared spectroscopy. *Kirk-Othmer Encyclopedia of Chemical Technology* **2000**, 1-18.

[18] Bhargava, R. Towards a practical Fourier transform infrared chemical imaging protocol for cancer histopathology. *Analytical and bioanalytical chemistry* **2007**, *389*, 1155-1169.

[19] Lasch, P.; Diem, M.; Hänsch, W.; Naumann, D. Artificial neural networks as supervised techniques for FT-IR microspectroscopic imaging. *Journal of Chemometrics: A Journal of the Chemometrics Society* **2006**, *20*, 209-220.

[20] Bellisola, G.; Sorio, C. Infrared spectroscopy and microscopy in cancer research and diagnosis. *Am. J. Cancer. Res.* **2012**, *2*, 1-21.

[21] Hammody, Z.; Argov, S.; Sahu, R. K.; Cagnano, E.; Moreh, R.; Mordechai, S. Distinction of malignant melanoma and epidermis using IR micro-spectroscopy and statistical methods. *Analyst* **2008**, *133*, 372-378. DOI: 10.1039/b712040k.

[22] Kosoglu, M. A.; Tata, D. B.; Ilev, I. K.; Hassan, M. Developing Test Methodology to Identify Intrinsic Biomarkers in Biological Models Using Fourier Transform Infrared (FTIR) Spectroscopy. *IEEE Journal on Selected Topics in Quantum Electronics* **2017**, *23* DOI: 10.1109/JSTQE.2016.2525723.

[23] Ghimire, H.; Venkataramani, M.; Bian, Z.; Liu, Y.; Perera, A. G. U. ATR-FTIR spectral discrimination between normal and tumorous mouse models of lymphoma and melanoma from serum samples. *Scientific Reports* **2017**, *7*, 16993. DOI: 10.1038/s41598-017-17027-4.

[24] Penaranda, F.; Naranjo, V.; Lloyd, G. R.; Kastl, L.; Kemper, B.; Schnekenburger, J.; Nallala, J.; Stone, N. Discrimination of skin cancer cells using Fourier transform infrared spectroscopy. *Comput. Biol. Med.* **2018**, *100*, 50-61. DOI: 10.1016/j.compbiomed.2018.06.023.

[25] Hammody, Z.; Sahu, R. K.; Mordechai, S.; Cagnano, E.; Argov, S. Characterization of malignant melanoma using vibrational spectroscopy. *Thescientificworldjournal* **2005**, *5*, 173-182. DOI: 10.1100/tsw.2005.1.

[26] Mordechai, S.; Sahu, R. K.; Hammody, Z.; Mark, S.; Kantarovich, K.; Guterman, H.; Podshyvalov, A.; Goldstein, J.; Argov, S. Possible common biomarkers from FTIR microspectroscopy of cervical cancer and melanoma. *J. Microsc.* **2004**, *215*, 86-91. DOI: 10.1111/j.0022-2720.2004.01356.x.

[27] Tfayli, A.; Piot, O.; Durlach, A.; Bernard, P.; Manfait, M. Discriminating nevus and melanoma on paraffin-embedded skin biopsies using FTIR micro spectroscopy. *Biochimica Et Biophysica Acta-General Subjects* **2005**, *1724*, 262-269. DOI: 10.1016/j.bbagen.2005.04.020.

[28] Tosi, G.; Conti, C.; Giorgini, E.; Ferraris, P.; Garavaglia, M. G.; Sabbatini, S.; Staibano, S.; Rubini, C. FTIR microspectroscopy of melanocytic skin lesions: a preliminary study. *Analyst* **2010**, *135*, 3213-3219. DOI: 10.1039/c0an00505c.

[29] Giorgini, E.; Tosi, G.; Conti, C.; Staibano, S.; Ilardi, G.; Sabbatini, S. FTIR microspectroscopic characterization of Spitz nevi. *Spectrochimica Acta Part A-Molecular and Biomolecular Spectroscopy* **2015**, *141*, 99-103. DOI: 10.1016/j.saa.2015.01.052.

[30] Ly, E.; Cardot-Leccia, N.; Ortonne, J. -.; Benchetrit, M.; Michiels, J. -.; Manfait, M.; Piot, O. Histopathological characterization of primary cutaneous melanoma using infrared microimaging: a proof-of-concept study. *Br. J. Dermatol.* **2010**, *162*, 1316-1323. DOI: 10.1111/j.1365-2133.2010.09762.x.

[31] Wald, N.; Goormaghtigh, E. Infrared imaging of primary melanomas reveals hints of regional and distant metastases. *Analyst* **2015**, *140*, 2144-2155. DOI: 10.1039/c4an01831a.

[32] Wald, N.; Bordry, N.; Foukas, P. G.; Speiser, D. E.; Goormaghtigh, E. Identification of melanoma cells and lymphocyte subpopulations in lymph node metastases by FTIR imaging histopathology. *Biochimica Et Biophysica Acta-Molecular Basis of Disease* **2016**, *1862*, 202-212. DOI: 10.1016/j.bbadis.2015.11.008.

[33] Minnes, R.; Nissinmann, M.; Maizels, Y.; Gerlitz, G.; Katzir, A.; Raichlin, Y. Using Attenuated Total Reflection-Fourier Transform Infra-Red (ATR-FTIR) spectroscopy to distinguish between melanoma cells with a different metastatic potential. *Scientific Reports* **2017**, *7*, 4381. DOI: 10.1038/s41598-017-04678-6.

[34] Ukkonen, H.; Kumar, S.; Mikkonen, J.; Salo, T.; Singh, S. P.; Koistinen, A. P.; Goormaghtigh, E.; Kullaa, A. M. Changes in the microenvironment of invading melanoma and carcinoma cells identified by FTIR imaging. *Vibrational Spectroscopy* **2015**, *79*, 24-30. DOI: 10.1016/j.vibspec.2015.04.005.

[35] Kong, R.; Reddy, R. K.; Bhargava, R. Characterization of tumor progression in engineered tissue using infrared spectroscopic imaging. *Analyst* **2010**, *135*, 1569-1578. DOI: 10.1039/c0an00112k [doi].

[36] Verdonck, M.; Wald, N.; Janssis, J.; Yan, P.; Meyer, C.; Legat, A.; Speiser, D. E.; Desmedt, C.; Larsimont, D.; Sotirioud, C.; Goormaghtigh, E. Breast cancer and melanoma cell line identification by FTIR imaging after formalin-fixation and paraffin-embedding. *Analyst* **2013**, *138*, 4083-4091. DOI: 10.1039/c3an00246b.

[37] Zwielly, A.; Gopas, J.; Brkic, G.; Mordechai, S. Discrimination between drug-resistant and non-resistant human melanoma cell lines by FTIR spectroscopy. *Analyst* **2009**, *134*, 294-300. DOI: 10.1039/b805223a.

[38] Zwielly, A.; Mordechai, S.; Brkic, G.; Bogomolny, E.; Pelly, I. Z.; Moreh, R.; Gopas, J. Grading of intrinsic and acquired cisplatin-resistant human melanoma cell lines: an infrared ATR study. *European Biophysics Journal with Biophysics Letters* **2011**, *40*, 795-804. DOI: 10.1007/s00249-011-0695-2.

[39] Wald, N.; Le Corre, Y.; Martin, L.; Mathieu, V.; Goormaghtigh, E. Infrared spectra of primary melanomas can predict response to chemotherapy: The example of dacarbazine. *Biochimica Et Biophysica Acta-Molecular Basis of Disease* **2016**, *1862*, 174-181. DOI: 10.1016/j.bbadis.2015.10.030.

[40] Acerbo, A. S.; Miller, L. M. Assessment of the chemical changes induced in human melanoma cells by boric acid treatment using infrared imaging. *Analyst* **2009**, *134*, 1669-1674. DOI: 10.1039/b823234b [doi].

[41] Srisayam, M.; Weerapreeyakul, N.; Barusrux, S.; Tanthanuch, W.; Thumanu, K. Application of FTIR microspectroscopy for characterization of biomolecular changes in human melanoma cells treated by sesamol and kojic acid. *J. Dermatol. Sci.* **2014**, *73*, 241-250. DOI: 10.1016/j.jdermsci.2013.11.002.

[42] Khanmohammadi, M.; Nasiri, R.; Ghasemi, K.; Samani, S.; Garmarudi, A. B. Diagnosis of basal cell carcinoma by infrared spectroscopy of whole blood samples applying soft independent modeling class analogy. *J. Cancer Res. Clin. Oncol.* **2007**, *133*, 1001-1010. DOI: 10.1007/s00432-007-0286-x.

[43] Khanmohammadi, M.; Garmarudi, A. B.; Ghasemi, K. Back-propagation artificial neural network and attenuated total reflectance-Fourier transform infrared spectroscopy for diagnosis of basal cell carcinoma by blood sample analysis. *J. Chemometrics* **2009**, *23*, 538-544. DOI: 10.1002/cem.1250.

[44] Khanmohammadi, M.; Ghasemi, K.; Garmarudi, A. B. Genetic algorithm spectral feature selection coupled with quadratic discriminant analysis for ATR-FTIR spectrometric diagnosis of basal cell carcinoma via blood sample analysis. *Rsc Advances* **2014**, *4*, 41484-41490. DOI: 10.1039/c4ra04965a.

[45] Wong, P. T.; Goldstein, S. M.; Grekin, R. C.; Godwin, T. A.; Pivik, C.; Rigas, B. Distinct infrared spectroscopic patterns of human basal cell carcinoma of the skin. *Cancer Res.* **1993**, *53*, 762-765.

[46] Ly, E.; Piot, O.; Wolthuis, R.; Durlach, A.; Bernard, P.; Manfait, M. Combination of FTIR spectral imaging and chemometrics for tumour detection from paraffin-embedded biopsies. *Analyst* **2008**, *133*, 197-205. DOI: 10.1039/b715924b.

[47] McIntosh, L. M.; Jackson, M.; Mantsch, H. H.; Stranc, M. F.; Pilavdzic, D.; Crowson, A. N. Infrared spectra of basal cell carcinomas are distinct from non-tumor-bearing skin components. *J. Invest. Dermatol.* **1999**, *112*, 951-956. DOI: 10.1046/j.1523-1747.1999.00612.x.

[48] Bortoletto, D. R.; Lima, C. A.; Zezell, D.; Sato, E. T.; Martinho, H. Vibrational spectra calculation of squamous cell carcinoma in the amide band region. *Vibrational Spectroscopy* **2018**, *97*, 135-139. DOI: 10.1016/j.vibspec.2018.06.007.

[49] Lima, C. A.; Goulart, V. P.; Correa, L.; Pereira, T. M.; Zezell, D. M. ATR-FTIR Spectroscopy for the Assessment of Biochemical Changes in Skin Due to Cutaneous Squamous Cell Carcinoma. *International Journal of Molecular Sciences* **2015**, *16*, 6621-6630. DOI: 10.3390/ijms16046621.

[50] Ly, E.; Piot, O.; Durlach, A.; Bernard, P.; Manfait, M. Differential diagnosis of cutaneous carcinomas by infrared spectral micro-imaging combined with pattern recognition. *Analyst* **2009**, *134*, 1208-1214. DOI: 10.1039/b820998g.

[51] Crupi, V.; Galli, S.; Majolino, D.; Migliardo, P.; Pergolizzi, S.; Venuti, V. Recent results on biomedical problems: A Fourier transform infrared (FT-IR) study. *Spectroscopy* **2002**, *16*, 245-250. DOI: 10.1155/2002/643587.

[52] Sebiskveradze, D.; Vrabie, V.; Gobinet, C.; Durlach, A.; Bernard, P.; Ly, E.; Manfait, M.; Jeannesson, P.; Piot, O. Automation of an algorithm based on fuzzy clustering for analyzing tumoral heterogeneity in human skin carcinoma tissue sections. *Laboratory Investigation* **2011**, *91*, 799-811. DOI: 10.1038/labinvest.2011.13.

[53] Kyriakidou, M.; Anastassopoulou, J.; Tsakiris, A.; Koui, M.; Theophanides, T. FT-IR Spectroscopy Study in Early Diagnosis of Skin Cancer. *In Vivo* **2017**, *31*, 1131-1137. DOI: 10.21873/invivo.11179.

[54] Wald, N.; Legat, A.; Meyer, C.; Speiser, D. E.; Goormaghtigh, E. An infrared spectral signature of human lymphocyte subpopulations from peripheral blood. *Analyst* **2015**, *140*, 2257-2265. DOI: 10.1039/c4an02247e.

[55] Chew, S. F.; Wood, B. R.; Kanaan, C.; Browning, J.; MacGregor, D.; Davis, I. D.; Cebon, J.; Tait, B. D.; McNaughton, D. Fourier transform infrared imaging as a method for detection of HLA class I expression in melanoma without the use of antibody. *Tissue Antigens* **2007**, *69*, 252-258. DOI: 10.1111/j.1399-0039.2006.00775.x.

[56] Holman, H. N.; Martin, M. C.; Blakely, E. A.; Bjornstad, K.; McKinney, W. R. IR spectroscopic characteristics of cell cycle and cell death probed by synchrotron radiation based Fourier transform IR spectromicroscopy. *Biopolymers: Original Research on Biomolecules* **2000**, *57*, 329-335.

[57] Whelan, D. R.; Bambery, K. R.; Puskar, L.; McNaughton, D.; Wood, B. R. Synchrotron Fourier transform infrared (FTIR) analysis of single living cells progressing through the cell cycle. *Analyst* **2013**, *138*, 3891-3899.

[58] Duffy, M. J. The biochemistry of metastasis. In *Advances in clinical chemistry*Elsevier: 1996; Vol. 32, pp 135-166.

[59] Tandler, N.; Mosch, B.; Pietzsch, J. Protein and non-protein biomarkers in melanoma: a critical update. *Amino Acids* **2012**, *43*, 2203-2230.

[60] Belter, B.; Haase-Kohn, C.; Pietzsch, J. Biomarkers in Malignant Melanoma: Recent Trends and Critical Perspective. In *Cutaneous Melanoma: Etiology and Therapy*; Ward, W. H., Farma, J. M., Eds.; Brisbane (AU), 2017; .

Table 1: Characteristics of included studies arranged in the order of appearance in the results section

Author (Year)	Sample information				Substrate used	Mode	Pre-processing	Algorithms	Major findings
	Origin (Type)	Arrangement	Thick-ness	Quantity					
Hammody *et al.* (2008)	Human (Biopsies)	FFPE (Deparaffinized prior to measurement)	10µm	SSM: 55	ZnSe	Transmission	BC, Norm.	SM-MATLAB, DCF	Identified important biomarkers in the FTIR spectra of skin tissues and differentiated melanoma from surrounding epidermis with high specificity and sensitivity.
Kosoglu *et al.* (2017)	Human (Cultured cell lines)	Cell pellets placed on substrate and dried	NA	Not mentioned	CaF_2	Transmission	Norm., SG filter (9 points)	HCA	The change in FTIR absorption spectra in malignant cells may be related to increase in production of endogenous H_2O_2.
Ghimire *et al.* (2017)	Mouse (Serum)	1µl deposited on crystal surface and dried	NA	Subcutaneous melanoma: 8 Control: 15	Diamond crystal	ATR	Norm.	Student's t-test, deconvolution, HCA	The study showed remarkable differences between the ATR-FTIR spectra of serum samples representing tumour-bearing mouse models of melanoma from their control types.
Penaranda *et al.* (2018)	Human and mouse (Cultured cell lines)	Cultured cell lines grown on CaF_2 fixed with glutaraldehyde, dehydrated in an ascending	NA	Non tumoral: 6 (human: 3; mouse: 3) MM: 6 (human; from 3 batches)	CaF_2	Transmission	Norm., SNV, DiffSG, RMieS-EMSC	LDA, QDA and PLS-DA	Algorithms trained and tested with cell spectra from the same batch gives excellent discrimination but when cells from different batches are mixed to construct the algorithms the discrimination is poor. There is strong influence of sample preparation on results and comparability of cell FTIR spectra.

		ethanol series and air-dried.							
Hammody *et al.* (2005)	Human (Biopsies)	FFPE (Deparaffinized prior to measurement)	10µm	SSM: 10 Nevus: 20 Epidermis: 30	ZnSe	Transmission	BC, Norm.	T-test	For identification of melanoma and distinction from nevus, not only the ratios but also the shifts in peaks would play a role.
Mordechai *et al.* (2004)	Human (Biopsies)	FFPE (Deparaffinized prior to measurement)	10µm	SSM: 7 Nevi: 7	ZnSe	Transmission	BC, Norm.	Univariate analysis	RNA/DNA ratio measured at I(1121)/I(1020) shows higher values for malignant tissues.
Tfayli *et al.* (2005)	Human (Biopsies)	FFPE (Not deparaffinized prior to measurement)	10µm	Melanoma: 3 (LMM, SSM, ALM) Nevi: 3 (CN, JN)	ZnSe	Transmission	Norm.	HCA	The selection of the spectral zones for HCA is very important and can influence the results of clustering. Four spectral zones combined together corresponding to DNA and melanin can help to discriminate melanoma from nevi.
Tosi *et al.* (2010)	Human (Tissue)	FFPE (Deparaffinized prior to measurement)	6-7µm	Control skin: 3 RN: 3; DN: 5; DysN: 7; MM: 6	BaF_2	Transmission	BC, Norm., 2nd derivative, PCA	UHCA, HCA, PCA, curve fitting	FTIR can discriminate various skin lesions by extracting the representative spectrum of a melanocyte. Melanin spectrum is difficult to isolate but specific bands of melanin can be identified in the spectra of melanocytes in number and intensity related to the particular skin lesion.
Giorgini *et al.* (2015)	Human (Surgical resection)	FFPE (Deparaffinized prior to measurement)	5-6µm	Control skin: 4 MM: 6; CSN: 6; DSN: 7; ASN: 7	BaF_2	Transmission	BC, Norm., 2nd derivative, CO_2 removal, WVC	UHCA, HCA, PCA, peak fitting	CSN melanocytes show a lower amount of H-bonded proteins and a high glycogen content, while changes in secondary structures of proteins are found in DSM and ASM melanocytes with lower level of glycogen. In MM

									melanocytes, a major content of β-structures is found together with intense transcriptional activity.
Ly *et al.* (2010)	Human (Tissue)	FFPE (Not deparaffinized prior to measurement)	10µm	Melanoma: 11 (SSM: 4; NM: 3; ALM: 1; SM: 1; melanoma on nevus: 2) benign nevus: 1	CaF_2	Transmission	WVC, CO_2 removal, Norm., 2nd derivative	KMC, HCA	FTIR imaging can identify spectroscopic markers of melanoma cells compared with normal epidermis. Differences in cell morphology and heterogenicity with different tumours can also be characterized.
Wald *et al.* (2015)	Human (Tissue microarray)	FFPE (Deparaffinized prior to measurement)	3-5µm	Total: 208 (melanoma at different stages: 128; regional or distant metastases: 64; healthy: 16). Used: 81	BaF_2	Transmission	WVC, CO_2 peak removal, BC, Norm.	Difference spectra, Student's t-test, PCA, MANOVA, PLS-DA, PLSR, ROC curve	PLS-DA models allow accurate identification of the main cell types present in these tissue sections. There is no significant difference between the IR spectra of melanoma cells in the primary tumours and in the metastases. The infrared spectra of primary tumours can differentiate patients at stage I or II from that of patients at stage III or IV.
Wald *et al.* (2016)	Human (Biopsies)	FFPE (Deparaffinized prior to measurement)	5µm	Metastatic melanoma: 34 Metastatic and non-metastatic lymph node: 8	BaF_2	Transmission	WVC, CO_2 peak removal, BC, Norm.	PCA, KMC, MANOVA, PLS-DA	The spectra of different cell types (erythrocytes, melanoma cells, endothelial cells, lymphocytes and connective tissue) in lymph nodes invaded by melanoma metastases have different spectral features and can be identified based on their infrared spectra. There is the possibility of identifying the presence of metastases through the impact they have on lymphocytes.

Minnes *et al.* (2017)	Human and mouse (Cell lines)	Placed directly on ATR crystal	NA	Mouse melanoma: 2 Human melanoma: 2	Ge crystal	ATR	Norm., curve fitting	Univariate analysis	The higher metastatic potential cells have higher absorption intensity of amide II and more high-density water molecules at the cell membrane's vicinity, which results in a higher level of fluidity of the plasma membrane compared to less metastatic cells and can be a marker for the metastatic capacity of the tumour cell.
Ukkonen *et al.* (2015)	Human (Cultured cell lines on top of 3D myoma disc)	FFPE (Deparaffinized prior to measurement)	4µm	Melanoma: 2	BaF_2	Transmission	BC, Norm., WVC, Mie scattering correction	PCA, UHCA, Student's t-test and Global fitting	The features present in the amide and collagen triplet regions could serve as spectral markers for cancer-induced modifications in the tissue microenvironment. The myoma model together with FTIR analysis may provide a biologically relevant system for cancer invasion research.
Kong *et al.* (2010)	Human and engineered tissue	FFPE (Deparaffinized prior to measurement)	5µm	Engineered tissue with melanoma: 7	BaF_2 (Engineered skin) Low-e slides (Human skin)	Transmission and transflection	Norm.	Comprehensive data map	Chemical changes associated with tumour-stromal interactions have been observed during the course of tumour growth and appear to influence a 50–100 µm region.
Verdonck *et al.* (2013)	Human (Cell lines)	FFPE (Deparaffinized prior to measurement)	3µm	Melanoma: 4	BaF_2	Transmission	WVC, CO2 peak removal, BC and Norm.	Difference spectra, MANOVA, HCA, PCA, PLS-DA	FFPE processing is responsible for small but significant modifications of the IR spectrum of cells. Nonetheless, distinctions between IR spectra of cellular subtypes are as accurate as before FFPE processing.

Zwielly *et al.* (2009)	Human (Cell lines)	5µl of sample placed on ZnSe and air-dried for 1 hour	10µm	GA cell samples: 50 GAC cell samples: 48	ZnSe	Transmission	BC, Norm.	PCA, unpaired t-test	FTIR microscopy can differentiate between parental melanoma cell and their cisplatin drug-resistant variant which are morphologically undistinguishable.
Zwielly *et al.* (2011)	Human (Cell lines)	4µl of sample placed on ZnSe and air-dried for 1 hour	10µm	GA and BG: 2 GAC and BGC: 2	ZnSe	ATR	BC, Norm.	Cluster analysis, discriminant classification function	ATR spectroscopy can differentiate between cisplatin resistance and sensitivity patterns of two independent human melanoma cell lines. The mechanisms of cisplatin resistance differ for different cell lines.
Wald *et al.* (2016)	Human (Tissue)	FFPE (Deparaffinized prior to measurement)	4µm	Primary melanoma: 12 (5 responders and 7 non-responders)	BaF_2	Transmission	WVC, CO2 peak removal, BC, Norm.	Student's t-test, PCA, MANOVA, PLS-DA, ROC curve	The examination of melanoma histological sections by FTIR can reveal the sensitivity of cancer to dacarbazine. The non-responding melanoma cells have far less lipids than the responding ones. The difference between the spectra of two groups also highlights changes in the amide I protein region and the nucleic acid region.
Acerbo *et al.* (2009)	Human (Cultured cells)	Slide placed directly into the cell culture media	NA	Total: 30 (six for each concentration of boric acid)	MirrIR slide	Transflection	Pre-processing mask, BC, 2^{nd} derivative, Norm.	PCA	Boric acid supplementation affects both the morphological and chemical composition of human melanoma cells. At low concentrations there are subtle differences in protein structure, while at high doses cell replication is slow and dose-dependent. Decrease in the nucleic acid/protein ratio and the presence of amide I spectral shifts with higher concentration of boric acid suggest induction of cell apoptosis.

Srisayam *et al.* (2014)	Human (Cultured cells)	Sample placed on the slide and dried	NA	One for each concentration of sesamol and kojic acid	Silver-doped glass slide	Reflection	EMSC	PCA, 2nd derivative, curve fitting, one-way ANOVA, Turkey test	Sesamol possesses a stronger anti-melanogenesis than kojic acid by inhibiting the tyrosinase activity resulting in decreasing melanin content. FTIR microspectroscopy can distinguish melanosome biochemical changes but not melanin content.
Khanmohammadi *et al.* (2007)	Human (Whole blood)	Placed directly on ATR crystal	NA	Total: 102 BCC: 32 Normal: 40 Validation set: 30	Crystal	ATR	Not mentioned	KNN, PCA, SIMCA	KNN and PCA cannot separate the two mentioned groups. Cancerous blood samples can be correctly discriminated from non-cancerous samples using soft independent modelling class analogy (SIMCA) with high sensitivity and specificity.
Khanmohammadi *et al.* (2009)	Human (Whole blood)	Placed on ATR base	NA	Total: 90 Calibration set: 20 (normal: 10 and BCC: 10) Validation set: 10 Test set: 60	Crystal	ATR	PCA	ANN	Back propagation artificial neural network (BP-ANN) can correctly separate blood samples from people affected by BCC from those of non-cancerous samples with high sensitivity and specificity. The architecture and modifier used for training the algorithms play a major role in differentiating cancer and normal samples.
Khanmohammadi *et al.* (2014)	Human (Whole blood)	Placed on ATR base	NA	Training set: 38 (normal: 18 and BCC: 20) Validation set: 15 (normal: 7 and BCC: 8) Test set: 75	Crystal	ATR	Not mentioned	QDA, GA-QDA	ATR-FTIR spectroscopy with GA-QDA chemometric technique is a reliable approach for the detection of BCC via blood sample analysis as it showed the best classification performance with highest sensitivity and specificity for all training, validation and test sets.

				(normal: 35 and BCC: 40)					
Wong *et al.* (1993)	Human (From excision)	Tissue placed between substrate by applying pressure	0.01mg	BCC: 10 Normal: 10	BaF_2 and α-quartz powder	Transmission	Not mentioned	3rd power derivative, univariate analysis	Infrared spectroscopy combined with high pressure can differentiate basal cell carcinoma from normal skin by analysing the obtained spectra from various regions.
Ly *et al.* (2008)	Human (Biopsies)	FFPE (No deparaffinized prior to measurement)	10µm	BCC: 10	CaF_2 and ZnSe	Transmission	WVC, CO_2 removal, Norm., PCA, EMSC	KMC, HCA	Running PCA on paraffin spectra improves the efficiency of EMSC for removing paraffin contribution. When combined with EMSC, KMC can be very powerful for the identification of tumours.
McIntosh *et al.* (1999)	Human (Biopsies)	FFPE (Deparaffinized prior to measurement)	7µm	BCC: 32 Melanocytic lesions: 5 SCC: 7	CaF_2	Transmission	Norm., 2nd derivative	Student's t-test, LDA	FTIR used in conjunction with sophisticated statistical analyses, such as LDA, allows a non-subjective examination and classification between various skin lesions. However, the classification of BCC subtypes is difficult.
Bortoletto *et al.* (2018)	Swiss mice (Tissue)	FFPE (Deparaffinized prior to measurement)	5µm	Healthy: 1 SCC: 1	MirrIR low-E coated slides	ATR	BC, Norm.	STmod (Computational model) based on Density functional Theory	Confined water plays no role in the amide region and protonated proline is responsible for the strong coupling between vibrations instead of water. The absorption of infrared radiation by amino acids of the skin is the main light-tissue interaction process in the fingerprint region.

Lima *et al.* (2015)	Swiss mice (Biopsies)	FFPE (Deparaffinized prior to measurement)	5µm	Normal: 13 Neoplasia: 13	MirrIR low-E coated slides	ATR	SG filter	2nd derivative, student's t-test, HCA	The difference in neoplastic lesions and normal tissue mainly occur in the wavenumbers associated with the protein content. ATR-FTIR spectroscopy provides a useful tool to complement histopathological analysis in the clinical routine for the diagnosis of SCC.
Ly *et al.* (2009)	Human (Biopsies)	FFPE (No deparaffinized prior to measurement)	10µm	BCC: 7; SCC: 7; Bowen's disease: 5; Control: 2	CaF_2	Transmission	WVC, CO_2 removal, EMSC	KMC, PCA, LDA	Working directly on the fingerprint region for the discriminant analysis brings the most reliable outcomes. Performing LDA directly without data reduction using PCA produce more convincing results for the differential diagnosis of cutaneous lesions.
Crupi *et al.* (2002)	Human (Tissue)	NA	20µm	Healthy: 1 Basalioma: 1 Epithelioma: 2	KBr pellets	Transmission	Norm., BC, deconvolution	Univariate analysis	The lipids of cellular membranes are the most involved in structural changes resulting from the presence of epithelioma and basalioma.
Sebiskveradze *et al.* (2002)	Human (Biopsies)	FFPE (No deparaffinized prior to measurement)	10µm	SCC: 3 BCC: 4 Bowen's disease: 6	CaF_2	Transmission	EMSC	KMC, HHAC, FCM	FCM clustering with optimal parameters derived from a redundancy-based algorithm is more powerful than classical 'hard' clustering (KM and hierarchical classification) to reveal biologically relevant information related to the tumour heterogeneity and invasiveness.
Kyriakidou *et al.* (2017)	Human (Biopsies)	Formalin-fixed without paraffin embedding	Not mentioned	BCC: 8 MM: 8 Nevus: 2	Not mentioned	ATR	Not mentioned	Deconvolution	The band at 1048 cm^{-1} in MM assigned to hyaluronic acid can be used as a "marker band" of MM as it discriminates melanoma from non-melanoma cancers due to the presence of many HA-chain breakages.
Wald *et al.* (2015)	Human (Blood)	Dried on BaF_2 slide	NA	Healthy: 6	BaF_2	Transmission	WVC, CO_2 peak removal,	Difference spectra,	FTIR has an ability to accurately identify CD4+ T cells and CD8+ T cells and can also quantify T reg in a different

							Norm., BC, signal-to-noise ratio filter	Student's t-test, PLS-DA, PLS-R, ANOVA	mix of immune cells which can aid in successful immunotherapy.
Chew *et al.* (2007)	Human (Biopsies)	FFPE (Deparaffinized prior to measurement)	4µm	MM: 8	Silver-coated/ tin oxide-overcoated infrared reflective glass	Reflection	Low and high intensity signal removal, Norm., 2nd derivative	UHCA, paired t-test	FTIR imaging enables the distinction of HLA-class-I-positive and -negative areas in melanoma, and the technique does not need to be facilitated by any antibody attachment, which comprises most of the cost in IHC staining.

Abbreviations:

NA: Not applicable, FFPE: Formalin fixed paraffin embedded, ATR: Attenuated total reflection, ZnSe: Zinc selenide, CaF_2: Calcium fluoride, BaF_2: Barium fluoride, Ge: Germanium, KBr: Potassium bromide

SSM: Superficial spreading melanoma, MM: Malignant melanoma, LMM: Lentiginous MM, ALM: Acrolentiginous melanoma, NM: Nodular melanoma, SM: Subcutaneous melanoma, CN: Composed nevus, JN: Junctional nevus, RN-Reed nevus, DN: Dermal nevus, DsyN: Dysplastic nevus, CSN: Classic nevus, DSN: Desmoplastic nevus, ASN: Atypical spitz nevus, GA: parental cell line (melanoma), GAC: Cisplatin resistant counterpart of GA, BG: parental cell line (melanoma), BGC: Cisplatin resistant counterpart of BG, BCC: Basal cell carcinoma, SCC: Squamous cell carcinoma

BC: Baseline correction, Norm.: Normalization, SG: Savitzky Golay, SNV: Standard normal variate, EMSC: Extended multiplicative signal correction, PCA: Principal component analysis, WVC: Water vapour correction, CO_2: Carbon dioxide

DCF: Discriminant classification function, HCA: Hierarchical cluster analysis, UHCA: Unsupervised hierarchical cluster analysis, HHAC: Hybrid hierarchical agglomerative clustering, FCM: Fuzzy C-means clustering, KMC: K-means clustering, KNN: K-nearest neighbour, LDA: Linear discriminant analysis, QDA: Quadratic discriminant analysis, GA-QDA: Genetic algorithm-quadratic discriminant analysis, PLS-DA: Partial least square discriminant analysis, PLSR: Partial least square regression, ANOVA: Analysis of variance, MANOVA: Multivariate analysis of variance, ROC: Receiver operating characteristics, SIMCA: Soft independent modelling class analogy, ANN: Artificial neural network

Table 2: Approximate positions of bands used for the diagnosis of skin cancers along with their associated bonds descended from included studies [21,23,25,28,35,37-39,41,42].

Wavenumber	Band	Associated bonds
966 cm^{-1}	DNA**	C–C/C–O stretching of deoxyribose-ribose vibration
970 cm^{-1}	Nucleic acids and* phosphorylated proteins	Symmetrical stretching mode of dianionic phosphate monoesters of phosphorylated proteins and cellular nucleic acids
996 cm^{-1}	RNA**	
1020 cm^{-1}	DNA**	C-O deoxyribose stretching
1033 cm^{-1}	Glucose***	C-O stretching carbohydrate, β-anomer
1056 cm^{-1}	Glycogen***	$\nu_s(PO_2-)$ absorbance of phosphodiesters of nucleic acids and the O-H stretching coupled with C-O bending of C-OH groups of carbohydrates
1076 cm^{-1}	Mannose***	C-O stretching carbohydrate α-anomer [ν (C-O)]
1081 cm^{-1}	Phosphate*	Symmetric stretching vibrations of nucleic acids and phospholipids [ν_s (PO_2-)]
1121 cm^{-1}	RNA**	C-O band of ribose
1230 cm^{-1}	DNA**	
1238 cm^{-1}	Phosphate*	Antisymmetric stretching vibrations of nucleic acids and phospholipids [ν_{as} (PO_2-)]
1244 cm^{-1}	RNA**	Asymmetrical phosphodiester vibrations of nucleic acids
1400 cm^{-1}	Protein*	Symmetric vibrations of carboxylate functional groups of the amino acid side chains and fatty acid [ν_s (C=O)]
1456 cm^{-1}	Lipid*	Symmetric CH_2 bending [δ_s (CH_2)]
1512 cm^{-1}	Tyrosine**	Usually hidden and resolved in 2nd derivative spectra
1536 cm^{-1}	Cytosine***	C–N and C–O bonds in nucleic acids
1544 cm^{-1}	Amide II*	C=O stretching vibration of peptide backbone and coupling of δ_{N-H} modes
1576 cm^{-1}	Thymine***	C–N and C–O bonds in nucleic acids
1622 cm^{-1}	Uracil***	C–N and C–O bonds in nucleic acids
1633 cm^{-1}	Guanine***	C–N and C–O bonds in nucleic acids

1639 cm^{-1}	Sub-band of amide I***	Parallel β-pleated sheet (amide I)
1648 cm^{-1}	Amide I*	C=O stretching vibration of peptide backbone and coupling of *v* (C-N) modes
1650 cm^{-1}	Sub-band of amide I***	*v*(C=O) amide I; α-helix
1682 cm^{-1}	Adenine***	C–N and C–O bonds in nucleic acids
1694 cm^{-1}	Sub-band of amide I***	Anti-parallel β-pleated sheet (amide I)
1740 cm^{-1}	Lipid*	C=O stretching vibrations of the ester functional groups in phospholipids [*v* (C=O)]
2852 cm^{-1}	Lipid*	Symmetric CH_2 stretching [v_s CH_2]
2871 cm^{-1}	Lipid*	Symmetric CH_3 stretching [v_sCH_2]
2923 cm^{-1}	Lipid*	Antisymmetric CH_2 stretching [$v_{as}CH_2$]
2958 cm^{-1}	Lipid*	Antisymmetric CH_3 stretching [$v_{as}CH_{2]}$
3080 cm^{-1}	Amide B*	Peptide protein [–NHCO-]
3300 cm^{-1}	Amide A*	Stretching vibration of N-H groups of proteins [*v*(N-H)]

Note: Presented are the approximate positions of the spectral bands. These bands positions may change depending upon the used sample type, sample preparation method and mode of measurement.

*Prominent spectral bands

**Usually hidden and can be resolved using second derivative spectra

***Hidden in prominent spectral bands and can be resolved using deconvolution or peak fitting

Figure 1

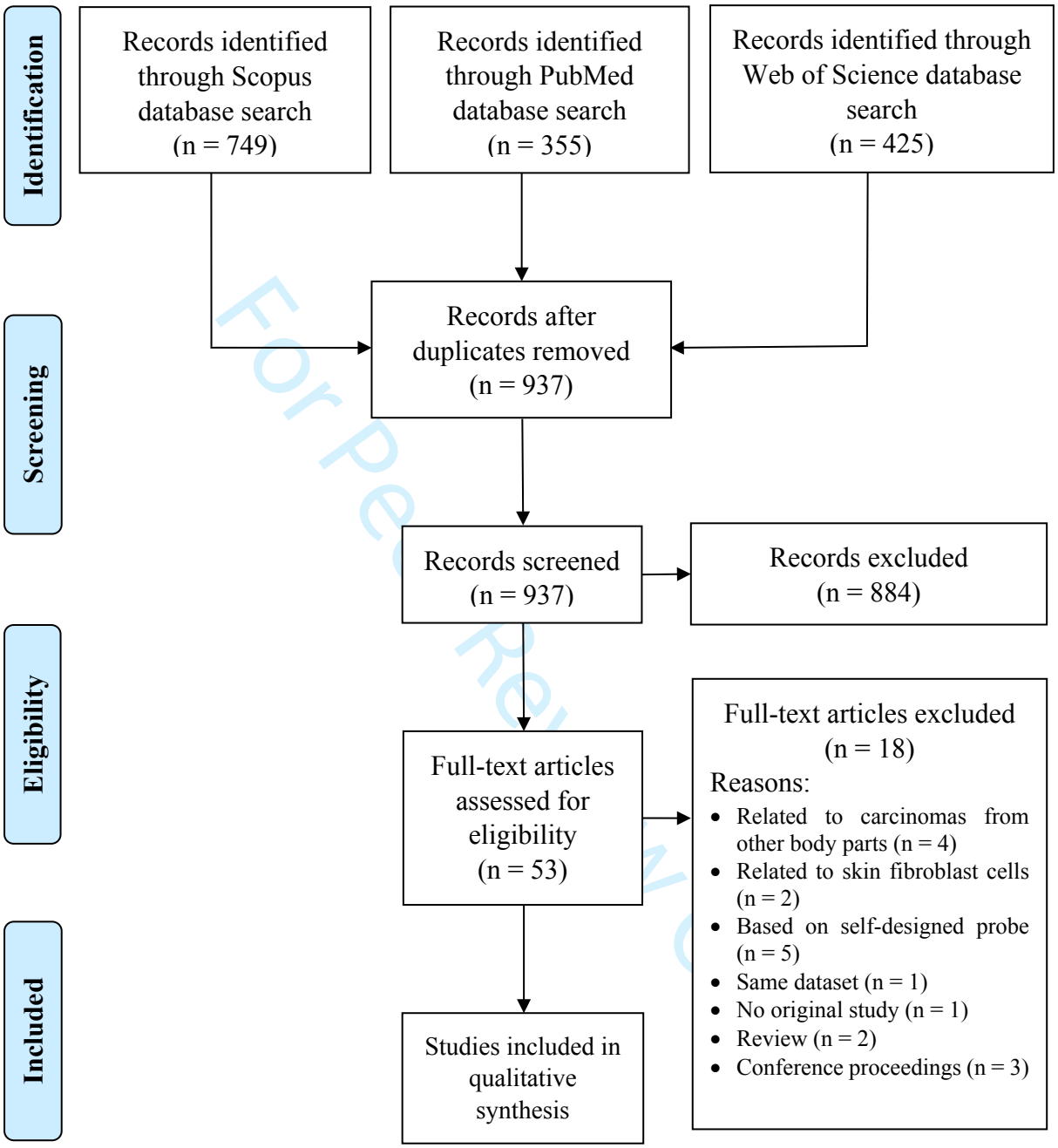

Figure captions

Figure 1: Flow diagram of selected studies.

Figure 2

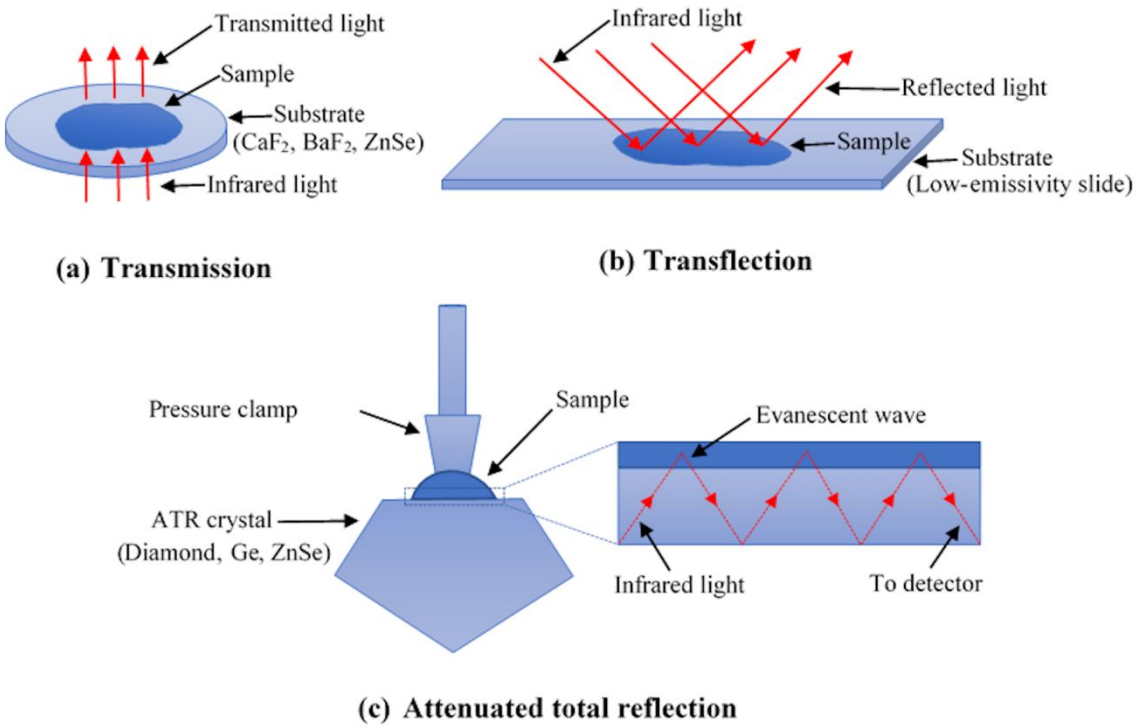

Figure captions

Figure 2: Schematic representation of the three different measurement modes in FTIR spectroscopy: a) transmission, b) transflection and c) attenuated total reflection (ATR). In ATR measurements, the pressure clamp is generally used for solid samples to ensure good contact with crystal but is not used in case of liquid samples.

Figure ~~23~~

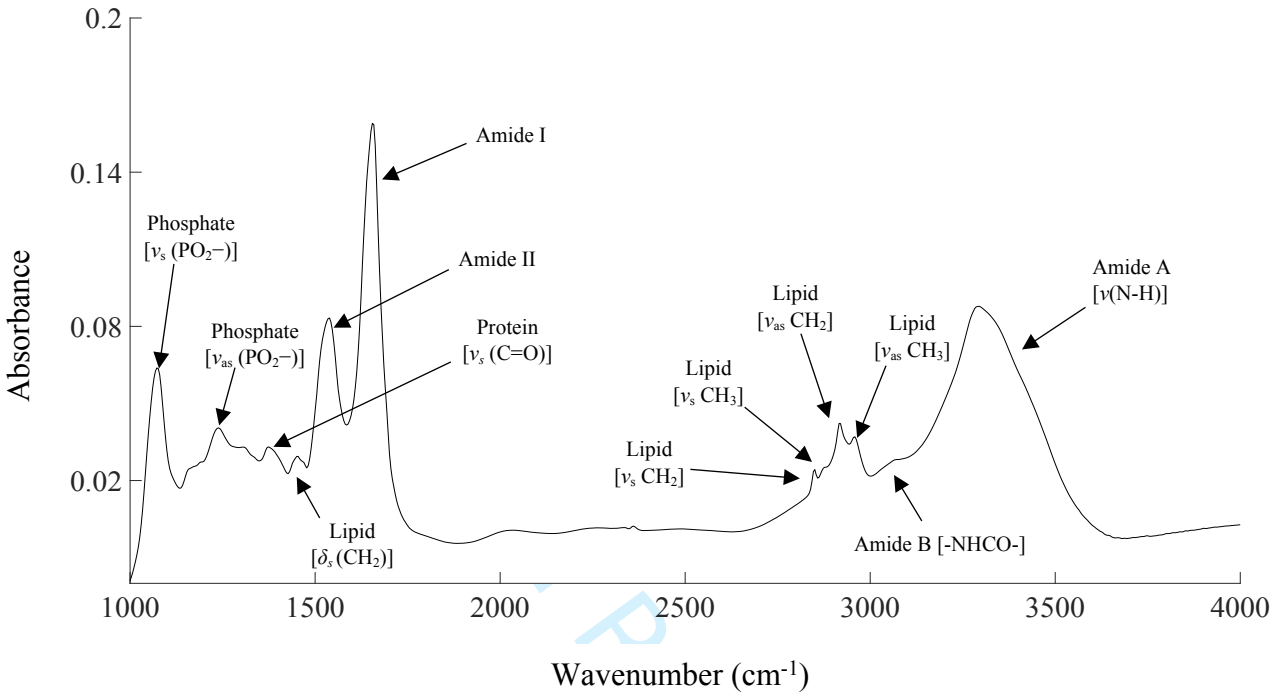

Figure captions

Figure ~~23~~: An infrared spectrum of a cultured metastatic melanoma cell (SK-MEL-30) with indicated prominent spectral bands.

Figure 4

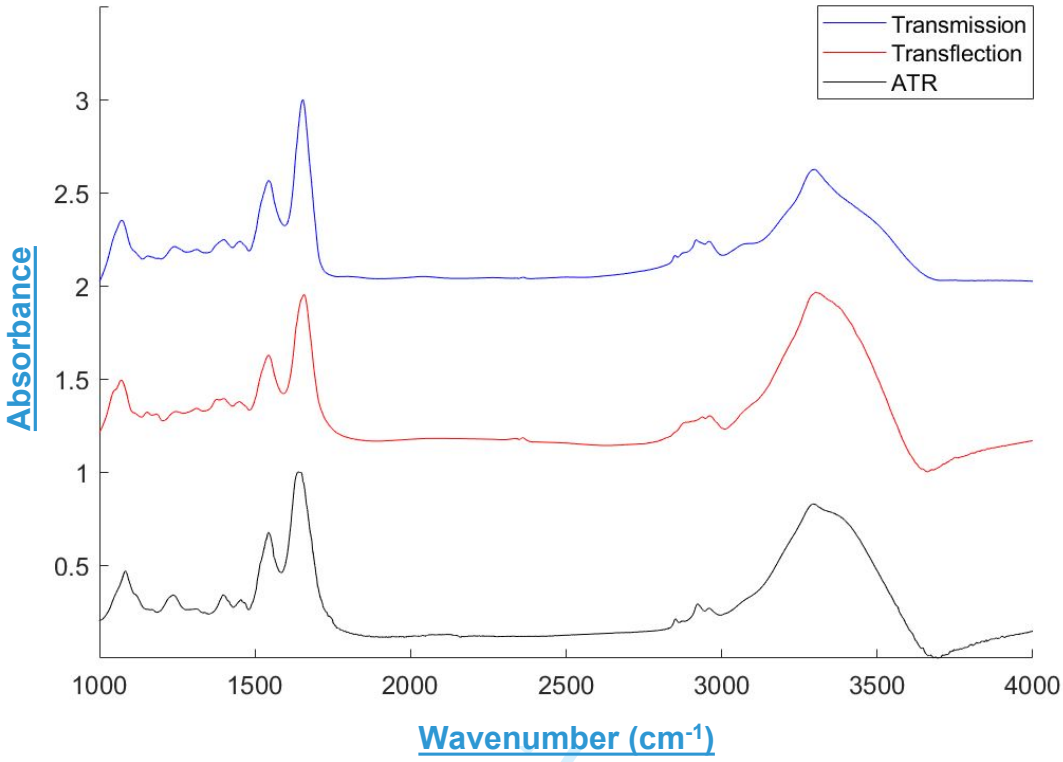

Figure captions

Figure 4: Infrared spectra of primary melanoma cells (IPC-298) acquired using different measurement modes of FTIR spectroscopy. For transmission and transflection, cultured cells were processed with FFPE protocol, and histological sections prepared from those were placed on CaF_2 and low-e slides, respectively. Furthermore, paraffin was removed before the measurements. For ATR measurements, live cells suspended in phosphate-buffered saline (PBS) were used. The ATR spectrum presented was obtained by subtracting pure PBS spectrum from the melanoma cell spectrum (both were measured after air drying). Offset values of one and two were added to transflection and transmission spectra, respectively, while plotting the figure to avoid overlap between the spectra.

Figure 35

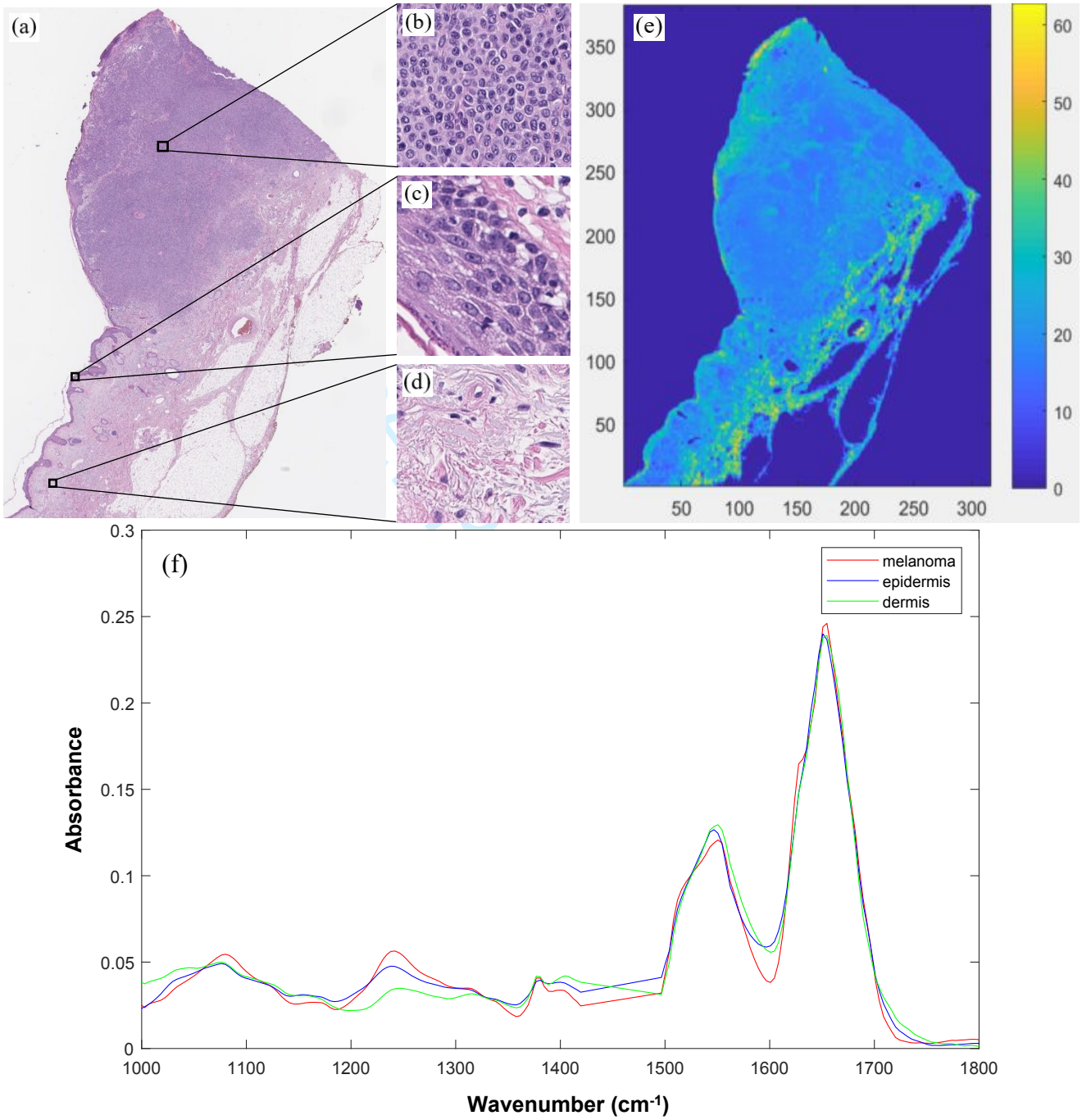

Figure caption

Figure 35: (a) Light microscopy image of a hematoxylin and eosin-stained melanoma biopsy sample and zoomed in images showing (b) melanoma cells, (c) normal epidermis, and

(d)dermis (e) FTIR image of an adjacent unstained section of the biopsy sample constructed using amide I absorbance and (f) averaged FTIR spectra from the regions b, c and d. The paraffin region (1420-1480 cm^{-1}) has been replaced by a straight line.

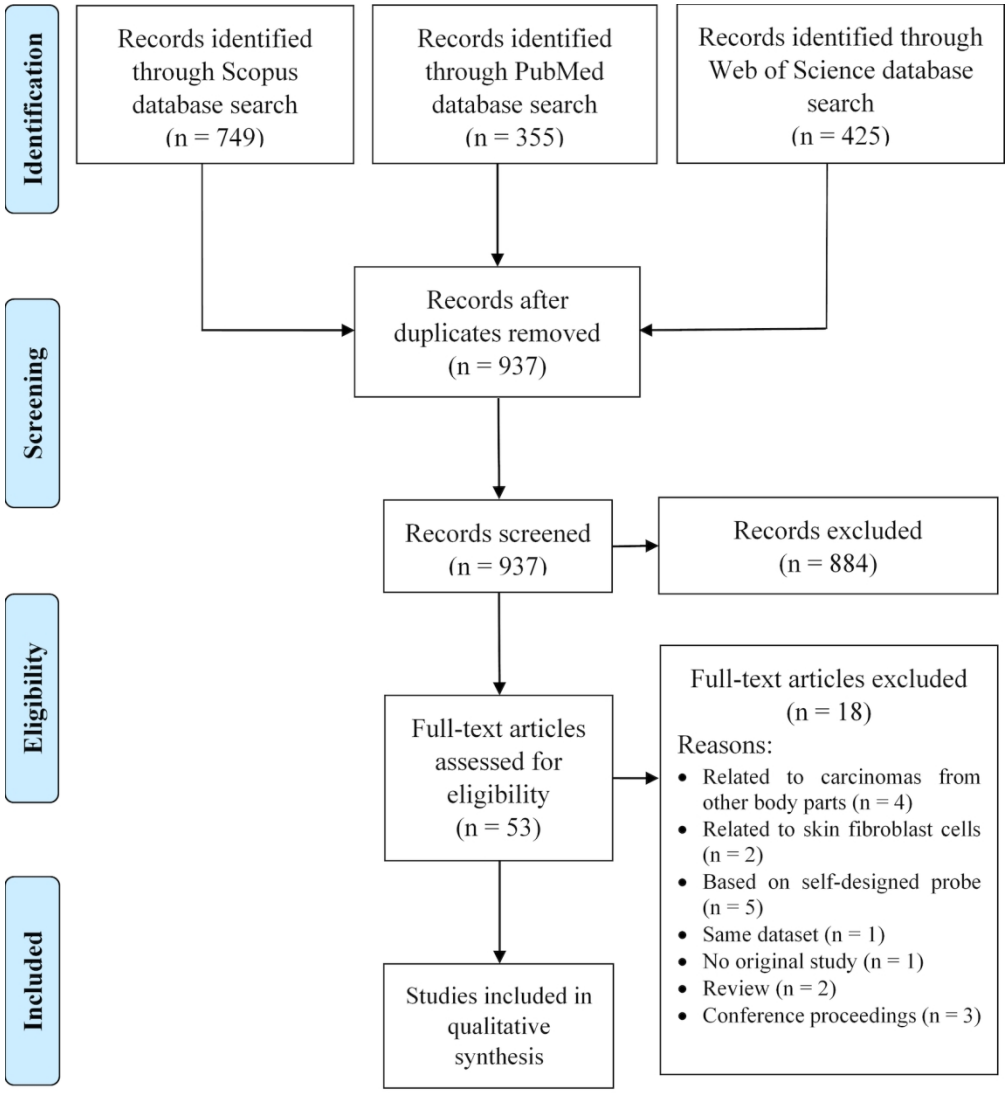

Flow diagram of selected studies.

150x165mm (300 x 300 DPI)

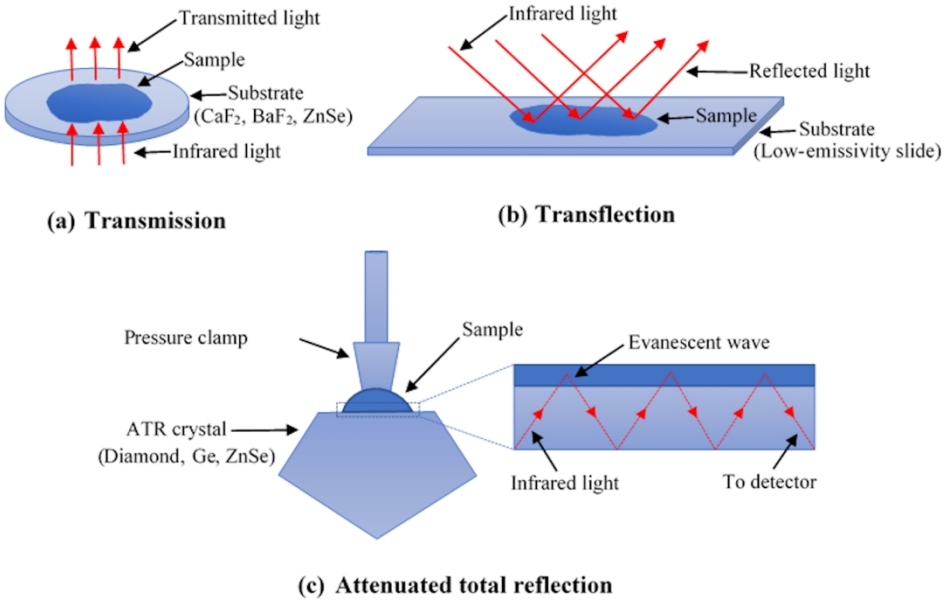

Schematic representation of the three different measurement modes in FTIR spectroscopy: a) transmission, b) transflection and c) attenuated total reflection (ATR). In ATR measurements, the pressure clamp is generally used for solid samples to ensure good contact with crystal but is not used in case of liquid samples.

160x105mm (300 x 300 DPI)

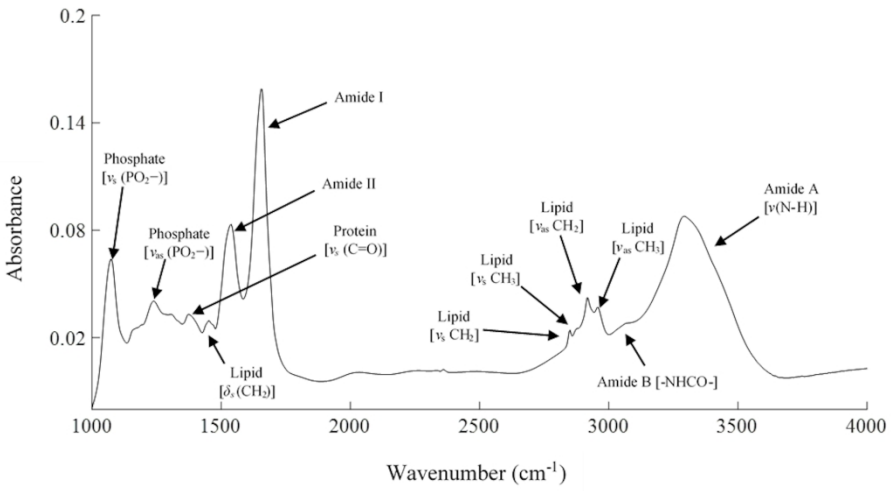

An infrared spectrum of a cultured metastatic melanoma cell (SK-MEL-30) with indicated prominent spectral bands.

189x97mm (300 x 300 DPI)

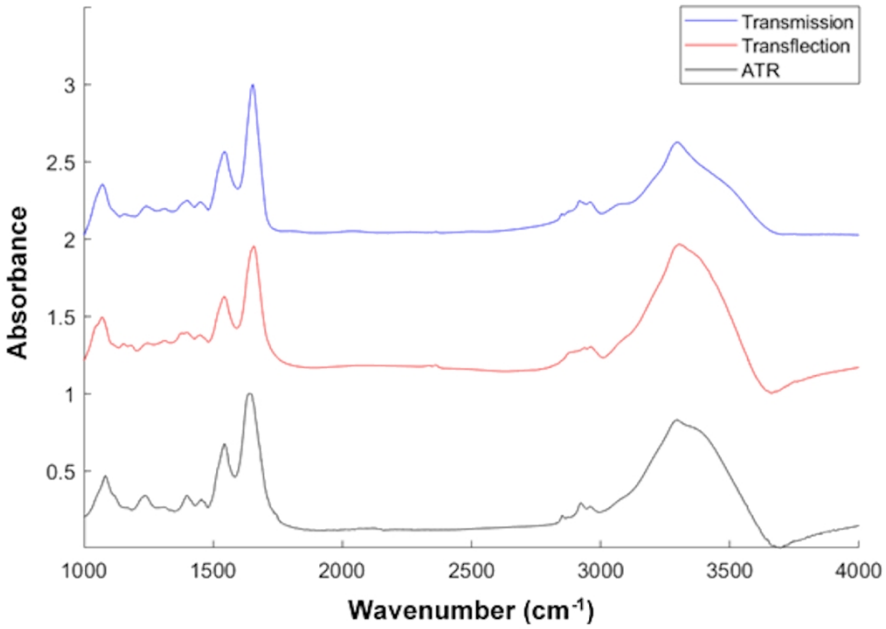

Infrared spectra of primary melanoma cells (IPC-298) acquired using different measurement modes of FTIR spectroscopy. For transmission and transflection, cultured cells were processed with FFPE protocol, and histological sections prepared from those were placed on CaF2 and low-e slides, respectively. Furthermore, paraffin was removed before the measurements. For ATR measurements, live cells suspended in phosphate-buffered saline (PBS) were used. The ATR spectrum presented was obtained by subtracting pure PBS spectrum from the melanoma cell spectrum (both were measured after air drying). Offset values of one and two were added to transflection and transmission spectra, respectively, while plotting the figure to avoid overlap between the spectra.

160x111mm (300 x 300 DPI)

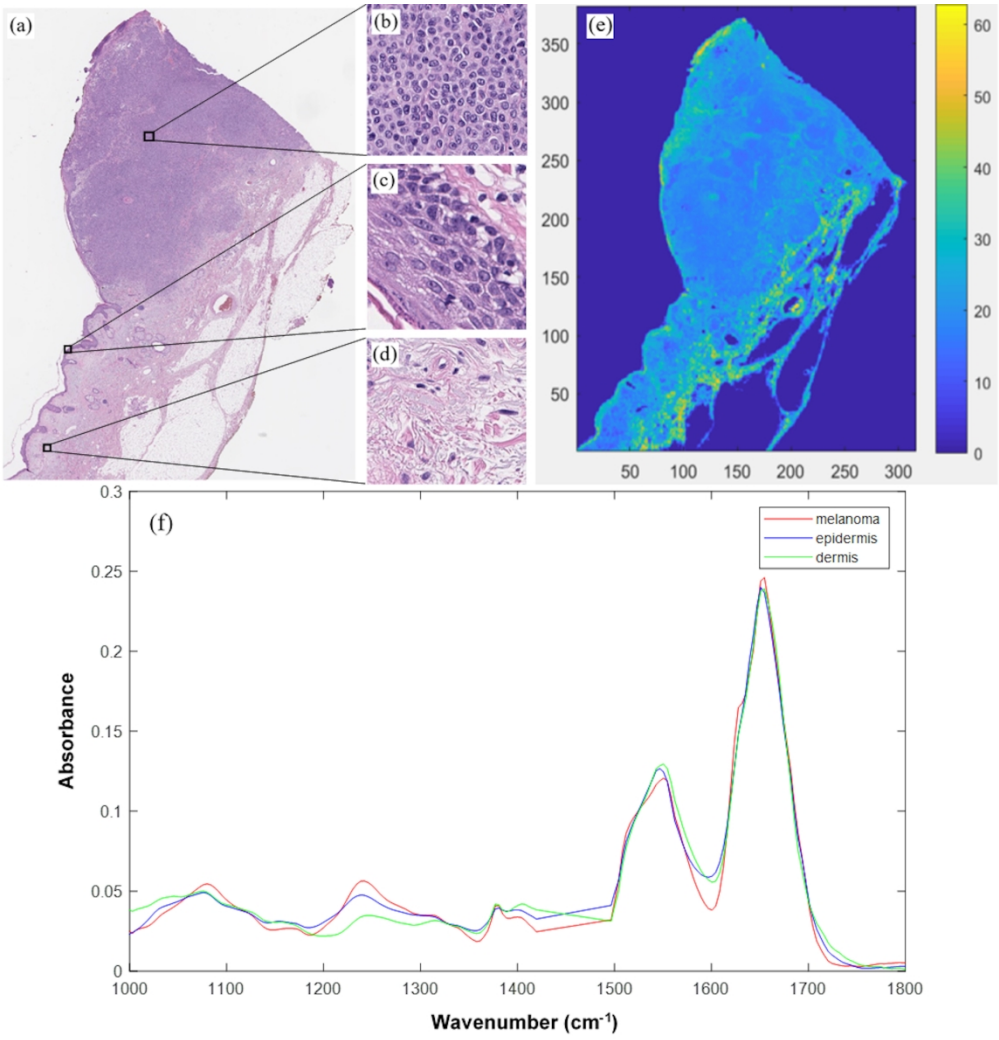

(a) Light microscopy image of a hematoxylin and eosin-stained melanoma biopsy sample and zoomed in images showing (b) melanoma cells, (c) normal epidermis, and (d)dermis (e) FTIR image of an adjacent unstained section of the biopsy sample constructed using amide I absorbance and (f) averaged FTIR spectra from the regions b, c and d. The paraffin region (1420-1480 cm-1) has been replaced by a straight line.

174x181mm (300 x 300 DPI)